

## Mechanisms of production of fast particles with $Z = 1, 2$ in ${}^6\text{Li}$ -induced reactions far above the Coulomb barrier

C. M. Castaneda,\* H. A. Smith, Jr.,† P. P. Singh, and H. Karwowski‡

Indiana University Cyclotron Facility and Physics Department, Bloomington, Indiana 47401

(Received 25 September 1978; revised manuscript received 30 May 1979)

Various mechanisms for the production of fast, beam-velocity particles have been explored using a 12.5 MeV/nucleon  ${}^6\text{Li}$  beam, with special emphasis on results from a  ${}^{197}\text{Au}$  target. Energy spectra and angular distributions of fast,  $Z = 1, 2$  products revealed an  $A^{1/3}$  target mass dependence of the individual total yields which is characteristic of the surface mechanisms. Relative fragment yields were essentially independent of the target mass and appear to depend upon the momentum distributions of the different cluster substructures of  ${}^6\text{Li}$ . Particle- $\gamma$  coincidences reflected the  $Q$ -optimum transfer of a beam-velocity  $\alpha$  or  $d$  fragment, initiating a (fragment,  $xn\gamma$ )-like reaction, and which accounts for approximately 13% of the singles beam-velocity particle production. In-plane  $\alpha$ - $d$  coincidences could be divided roughly equally between two-step (sequential) and one-step projectile breakup. Alpha-proton coincidences suggested the strong presence of neutron transfer, forming unstable  ${}^5\text{Li}$  which subsequently breaks up into  $\alpha + p$ . The cross section from correlated  $\alpha + d$  and  $\alpha + p$  production accounts for at least 50% of the singles fast-particle production. Other possible mechanisms are also discussed.

NUCLEAR REACTIONS  ${}^{197}\text{Au}, {}^{56}\text{Fe}({}^6\text{Li}, X) E = 75$  MeV, measured particle energy spectra and angular distributions.  ${}^{197}\text{Au}({}^6\text{Li}, X)$  measured two-dim  $\alpha$ - $d$ ,  $\alpha$ - $p$ ,  $\alpha$ - $\gamma$ ,  $d$ - $\gamma$ ,  $p$ - $\gamma$  coincident energy and angular correlations. Deduced  $\sigma_X(\theta)$ ,  $\sigma_{\text{tot}}(X)$ , reaction mechanisms.

### I. INTRODUCTION

The production of intense fluxes of fast  $\alpha$  particles in reactions involving complex nuclei has been a puzzle ever since the earliest heavy-ion experiments. In particular, beam-velocity  $\alpha$  particles were first observed in  ${}^{12}\text{C}$ ,  ${}^{14}\text{N}$ , and  ${}^{16}\text{O}$  bombardments,<sup>1</sup> where it was proposed that these particles arise from a fragmentation of the incident projectile in an interaction localized at the surface of the target nucleus. Some recent particle correlation measurements with a  ${}^{32}\text{S}$  beam<sup>2</sup> support the view that the fast  $\alpha$ -particle flux is emitted from the projectile rather than from the target nucleus. Other mechanisms for the production of fast  $\alpha$  particles have also been suggested, such as the well-known pre-equilibrium emission process<sup>3,4</sup> and a radial friction mechanism (the so-called "piston model").<sup>5</sup> Recent particle-particle angular correlation measurements<sup>2,6</sup> have not supported the radial friction picture but are instead more consistent with a mechanism involving *tangential* friction in the region of impact between target and projectile. Finally, it has also been proposed<sup>7</sup> that fast  $\alpha$  particles can arise from a three-body final-state process in which an  $\alpha$  particle is first transferred to the target at high excitation and then is re-emitted by the excited complex system.

The earliest experiments with low-energy  ${}^6\text{Li}$  beams also showed copious production of  $\alpha$  par-

ticles and the added feature of fast deuterons.<sup>8,9</sup> The energy spectra were similar to those seen in heavy-ion reactions: broad, bell-shaped peaks centered approximately at beam-velocity kinetic energies. These particles were generally interpreted as the outgoing fragments from the sequential breakup of the  ${}^6\text{Li}$ , Coulomb-excited to its 2.18-MeV  $3^*$  first excited state.

Many experiments have established that the  ${}^6\text{Li}$  nucleus has a well-developed cluster structure with significant  $\alpha + d$  amplitude<sup>10-13</sup> and also  ${}^3\text{He} + t$  amplitude.<sup>14</sup> More recent experiments<sup>15,16</sup> have determined that these amplitudes are approximately equal in magnitude, to within a factor of 2. The high degree of clustering in the Li ground states implies a significant probability that, when used as a projectile, these nuclei will often undergo binary dissociation into their cluster substructures. (Some studies involving  ${}^7\text{Li}$  have also been carried out,<sup>9,17,18</sup> but emphasis in the present work will be on the properties of  ${}^6\text{Li}$ .) This observation has led to the frequent use of Li ions in cluster-transfer studies, particularly those involving  $\alpha$  transfer.<sup>19-22</sup> In addition, many other experimental<sup>17,18,23-25</sup> and theoretical<sup>26-33</sup> studies of the lithium breakup phenomenon itself have been carried out. The work performed so far has largely been confined to sub- and near-Coulomb barrier beam energies, and the approaches have reflected the preoccupation with the  $\alpha + d$  dissociation of the  ${}^6\text{Li}$  as the source of

the particles.

Numerous experiments have also been performed utilizing the Li + target fusion-emission reactions and determining ( ${}^6,{}^7\text{Li}$ ,  $xny\beta z\alpha\dots$ ) cross sections by measuring the inclusive decay  $\alpha$ -particle<sup>34</sup> or  $\gamma$ -ray<sup>35-38</sup> spectra of the products. In the experiments cited, especially large yields were observed in the ( ${}^6,{}^7\text{Li}$ ,  $\alpha xn$ ), ( ${}^6\text{Li}$ ,  $dxn$ ), and ( ${}^7\text{Li}$ ,  $txn$ ) channels, relative to that expected from a fusion-emission mechanism alone. It has been suggested<sup>34,36-38</sup> that these results can be understood as arising from the dissociation of the incident projectile into its loosely bound cluster fragments, accompanied by the interaction of one of those clusters with the target nucleus.

Finally, data from particle coincidence measurements with  ${}^6\text{Li} + {}^{208}\text{Pb}$  near the Coulomb barrier<sup>23</sup> suggest the presence of still other  ${}^6\text{Li}$ -induced reaction mechanisms such as ( ${}^6\text{Li}$ ,  ${}^5\text{Li} \rightarrow \alpha + \beta$ ) and ( ${}^6\text{Li}$ ,  ${}^8\text{Be} \rightarrow \alpha + \alpha$ ), both of which produce fast  $\alpha$ -particle fluxes.

The present investigation was undertaken to ascertain the reaction mechanisms which produce fast particles in  ${}^6\text{Li}$  bombardments far above the Coulomb barrier, where the problem is enriched by the greater opportunity for prominence of nuclear interactions over Coulomb effects and where the full range of the reaction mechanisms discussed above must be considered. In this paper we describe measurements of charged-particle spectra and angular distributions from 75-MeV  ${}^6\text{Li}$  bombardments of several targets. In addition, particle-particle and particle- $\gamma$  correlations from 75-MeV bombardments of  ${}^{197}\text{Au}$  are described.

Detailed results will be considered only for the 75-MeV bombardment of  ${}^{197}\text{Au}$ . Data from runs with other targets are considered only in the exploration of the influence of the target nucleus on the particle yields.

Particular attention was paid to the understanding of the fast  $\alpha$ -particle flux since this flux was observed to be the most intense of all the particles and so would likely involve the greatest variety of reaction channels.

Preliminary reports of these measurements have already been made,<sup>39-41</sup> and the present work provides a detailed account of our results and interpretations.

## II. EXPERIMENTAL DETAILS AND GENERAL CONSIDERATIONS

Beams of fully ionized  ${}^6\text{Li}$  at energies of 75 MeV were obtained from the Indiana University Cyclotron Facility (IUCF). Beam currents utilized were typically in the 20-70 electrical nanoampere

range for the angular distribution and particle-particle correlation measurements and in the sub-nanoampere range for the particle- $\gamma$  coincidence runs. Charged-particle detection and identification was accomplished by means of two-element  $\Delta E$ - $E$  Si surface-barrier-detector telescopes consisting of 200 and 5000  $\mu\text{m}$  detectors, the total thickness chosen so as to stop completely the  $Z = 1, 2, 3$  particles in the energy ranges of interest. Gamma rays were detected by means of a 30  $\text{cm}^3$  coaxial Ge(Li) detector. In all runs, dead time corrections were determined by sending the output of a tail pulser (triggered by the outputs of the monitor counters) through the preamplifier test inputs of all of the detectors. The area of the resulting pulser peaks in the particle and  $\gamma$ -ray spectra were then compared with the reading of an external scaler which counted the number of pulser triggers.

Singles angular distribution measurements were performed at 75 MeV on  ${}^{56}\text{Fe}$ ,  ${}^{106}\text{Pd}$ , and  ${}^{197}\text{Au}$  targets. The particle- $\gamma$  measurements were carried out with  ${}^{56}\text{Fe}$  and  ${}^{197}\text{Au}$  targets, and the particle correlation experiments utilized only the  ${}^{197}\text{Au}$  target. All targets were fabricated in this laboratory. Target thicknesses were chosen in the 2-10  $\text{mg}/\text{cm}^2$  range in order to minimize the energy degradation and straggling of the beam and outgoing charged particles while allowing sufficient target thickness to generate acceptable data rates.

Singles data were stored, event by event, on magnetic tape, each event consisting of four parameters: the  $E_T$ ,  $E' = E_T - \Delta E$ , and  $\Delta E$  particle energy signals, and the particle ID signal. Particle identification was accomplished by means of hardware implementation of the algorithm<sup>42</sup>

$${}^{\text{ID}} \equiv MZ^2t = k_1\Delta E(E' + k_2\Delta E + k_3). \quad (1)$$

Particle- $\gamma$  and particle-particle coincidence spectra were acquired by means of the conventional fast-slow coincidence technique.

In the particle- $\gamma$  correlation measurements, the  $\gamma$ -ray detector was kept fixed in the reaction plane defined by the beam and particle detector axes and was oriented at  $90^\circ$  to the beam axis. The particle telescope was moved in  $5^\circ$  steps from  $10^\circ$  to  $50^\circ$ .

Six-parameter particle- $\gamma$  data consisted of  $E_T$ ,  $E'$ , and  $\Delta E$  particle detector and  $E_\gamma$   $\gamma$ -ray detector signals, the time distribution (TAC analog output) between  $E'$  and  $E_\gamma$  signals, and the particle ID signals.

The correlation runs were performed by fixing one of the detectors at  $25^\circ$  and moving the other telescope in steps of  $2^\circ$  from the minimum possible angular separation up to  $15^\circ$  relative separa-

tion. Also, measurements at positions of relative separation greater than  $15^\circ$  were obtained, with the moving telescope exploring both sides of the beam axis.

The particle-particle data consisted of seven signals,  $E_T$ ,  $\Delta E$ , and ID from each telescope and the TAC analog output.

The stability of the beam spot position as well as that of the beam charge integrator were checked through the use of two  $2000\ \mu\text{m}$  Si surface-barrier monitor detectors, placed at  $\pm 14.5^\circ$  (i.e., on opposite sides of the beam axis).

### III. EXPERIMENTAL RESULTS AND DISCUSSION

#### A. Singles spectra

Typical spectra of the outgoing charged particles observed in the present work are shown in Fig. 1 for bombardment of the  $^{197}\text{Au}$  target. All charged particles exhibit energy spectra in which essentially all of the intensity is concentrated in broad, structureless peaks centered at energies corresponding approximately to the beam velocity. In the bombardments of lighter targets (e.g.,  $^{56}\text{Fe}$ ) contributions to the spectra are also evident from the evaporation of  $\alpha$  particles and protons. The discussion in this work will focus, however, only on the characteristics of the fast (near-beam-velocity) particles and will deal primarily with results from  $^{197}\text{Au}$  bombardments, from which compound-nucleus charged-particle emission is greatly inhibited by the Coulomb barrier.

The angular distributions of the beam-velocity charged particles from the  $^{197}\text{Au}$  bombardment are shown in Fig. 2, where it is clear that the singles yields are concentrated in the forward angles. This forward-peaked character to the spectra is even more pronounced in the lighter targets, as evidenced in the fast-particle angular distributions for the  $^{56}\text{Fe}$  target, shown in Fig. 3. Integration of the angular distributions over the observed angular range (assuming azimuthal symmetry about the beam axis) gives the total yields of the fast charged particles, which are listed in Table I. These total yields and also relative yields (compared with the fast  $\alpha$ -particle production) are plotted in Figs. 4(a) and 4(b), respectively. It is clear from these results that there is a marked excess of  $\alpha$  particles over deuterons. Furthermore, the  $\alpha$  and  $d$  yields are more than an order of magnitude higher than the  $^3\text{He}$  and triton yields, and the triton yields are 2 to 3 times larger than the  $^3\text{He}$  yields. In the total particle yields [Fig. 4(a)] a preference is shown for an  $A_t^{1/3}$  dependence on target mass, characteristic of surface-peaked production mechanisms.

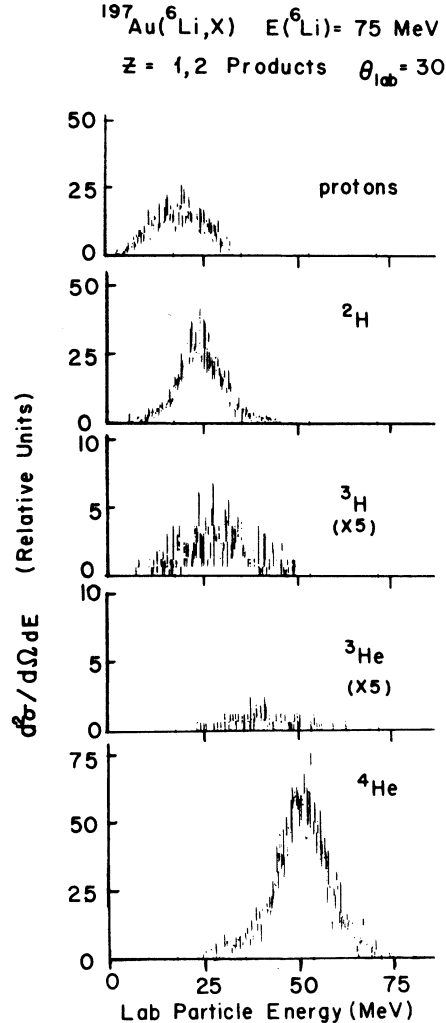
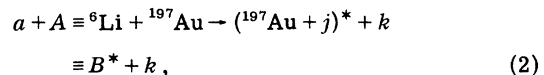


FIG. 1. Singles energy spectra of charged particles produced in the 75-MeV  $^6\text{Li}$  bombardment of  $^{197}\text{Au}$ . Note that the  $^3\text{He}$  and triton groups are displayed at 5 times the vertical gain of the other spectra.

In addition, the relative particle yields [Fig. 4(b)] tend to exhibit minimal dependence on target mass, suggesting that the particle production is more a reflection of the structure of the projectile than of the target.

The apparent surface-peaked nature of the particle production leads us to consider the singles energy spectra from bombardments of  $^{197}\text{Au}$  from the viewpoint of a multinucleon transfer, represented schematically by the reaction



where particle  $k$  is the observed outgoing charged particle, and  $j$  is the remainder of the  $^6\text{Li}$  which is transferred. The  $Q$  value for this process,

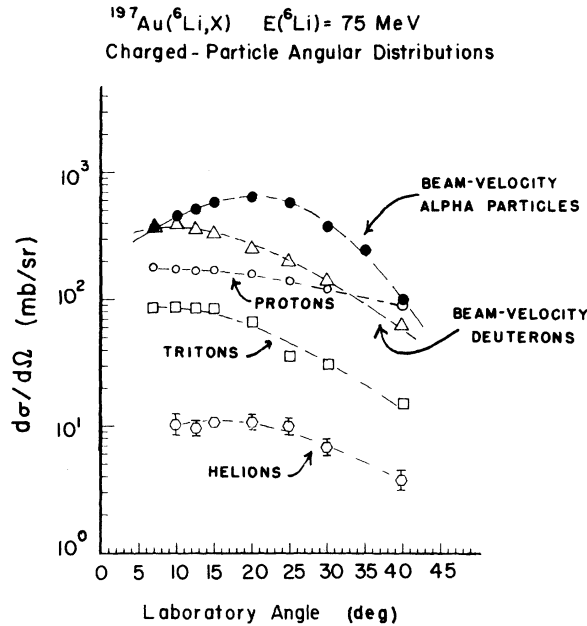


FIG. 2. Angular distributions of charged particles from the 75-MeV bombardment of  $^{197}\text{Au}$ .

defined in terms of center-of-mass kinetic energies, is

$$Q_k = E_B^{\text{CM}} + E_k^{\text{CM}} - E_A^{\text{CM}} - E_a^{\text{CM}}. \quad (3)$$

Momentum conservation allows a given value of  $E_k^{\text{CM}}$  (and hence  $E_k^{\text{lab}}$ ) to be associated with a unique  $Q$  value for the event, the balance of the outgoing kinetic energy being taken up by the recoil of the residual system  $B^*$ . Utilizing this strict kinematic relationship between  $E_k^{\text{lab}}$  and  $Q_k$ , we transform the  $30^\circ$   $^{197}\text{Au}(^6\text{Li}, X)$  outgoing fragment energy spectra in Fig. 1 into their corresponding  $Q$ -value spectra in Fig. 5(b). For purposes of comparison, we also show in Fig. 5(b) a similar  $Q$ -value plot for the same reaction for fragments at  $15^\circ$ .

The values of  $Q_k$  at which the energy spectra peak for each particle type  $k$  ( $\bar{Q}_k$ ) are observed to be independent of the angle of emission of the particle. Furthermore, comparison with the  $^{56}\text{Fe}$  spectra [Fig. 5(a)] indicates that the  $\bar{Q}_k$ 's are also essentially independent of the target used. It is well known in heavy-ion reactions that the reaction cross sections are greatly enhanced at an optimum  $Q$  value for which the incoming and outgoing channels are smoothly connected by classical angular momentum and energy conservation laws. Von Oertzen<sup>45</sup> has outlined a simple method for calculating these optimum  $Q$  values by making the physically reasonable requirement that continuous trajectories be ensured through invariance of the *radial* channel momen-

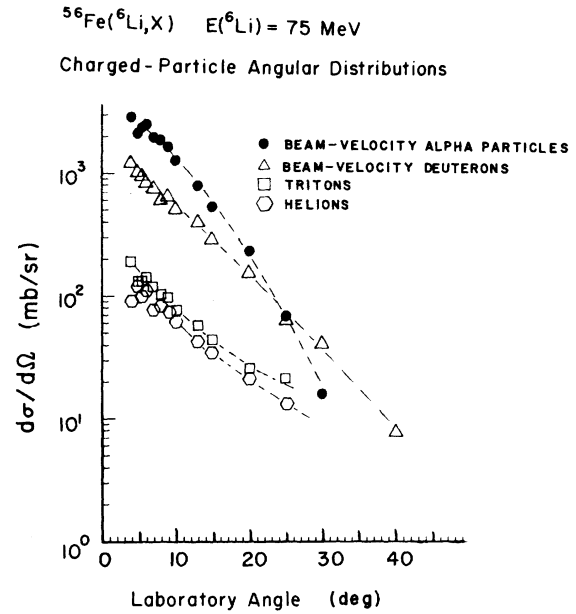


FIG. 3. Angular distributions of charged particles from the 75-MeV bombardment of  $^{56}\text{Fe}$ .

tum during the reaction. Under this restriction, the optimum  $Q$  value is attained by a balance of the Coulomb, nuclear, and angular momentum (centrifugal) potentials in the entrance and exit channels in the projectile-target center-of-mass system. The 75-MeV  $^6\text{Li} + ^{197}\text{Au}$  reaction has a Sommerfeld parameter  $\eta (= Z_1 Z_2 e^2 / \hbar v)$  of 10, which makes it appropriate to consider the reaction in such a semiclassical context. The optimum  $Q$  values (calculated as in Ref. 45) for the transfer of  $\Delta A_k$  nucleons (producing particle  $k$ ) are plotted *versus*  $\Delta A_k$  in Fig. 6 and compared with the measured  $\bar{Q}_k$ 's for this reaction. Also plotted for comparison are calculations for this same reaction at 95 and 154 MeV, and comparison is made with experimental results at these energies obtained by Vigdor and co-workers.<sup>46</sup>

TABLE I. Total production cross sections (in mb) for fast charged particles from 75-MeV  $^6\text{Li}$  bombardment of various targets (see Fig. 4).

Particle	$\sigma_1(^{56}\text{Fe} \text{ tgt})$	$\sigma_2(^{106}\text{Pd} \text{ tgt})$	$\sigma_3(^{197}\text{Au} \text{ tgt})$
$\alpha$	$287 \pm 32$	$399 \pm 60$	$569 \pm 66$
$d$	$167 \pm 19$	$205 \pm 30$	$259 \pm 29$
$^3\text{He}$	$16 \pm 3$	$20 \pm 3$	$20 \pm 4$
$t$	$22 \pm 4$	$40 \pm 6$	$59 \pm 12$
$\sigma_R^a$	1864	2151	2320

<sup>a</sup>Total reaction cross section calculated using the parabolic model (Ref. 43). This calculation was performed with the ALICE OVERLAID code of M. Blann (Ref. 44).

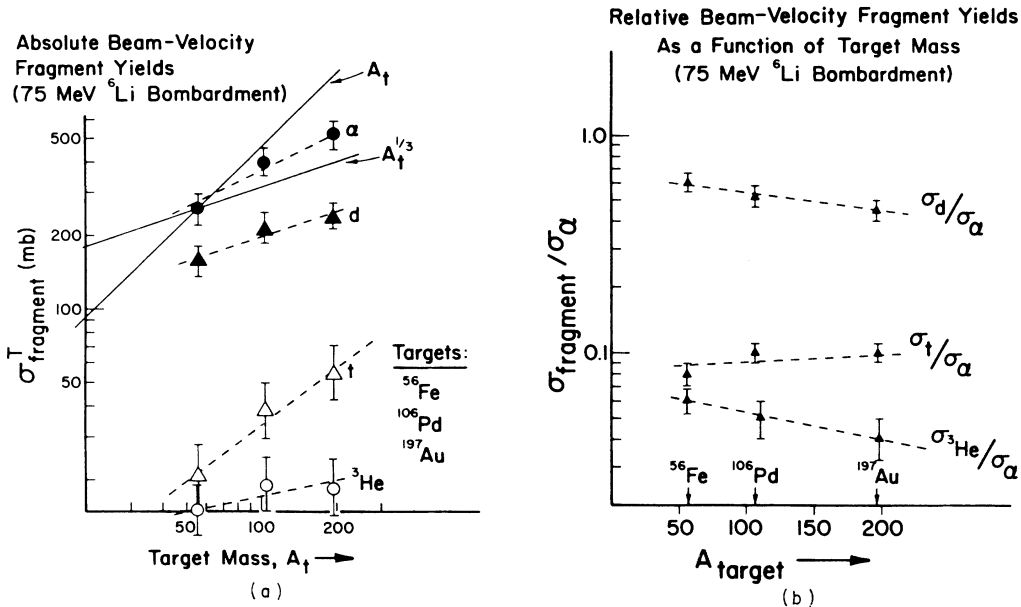


FIG. 4. (a) Total fast charged-particle yields from 75-MeV  ${}^6\text{Li}$  bombardments, shown as a function of target mass number,  $A_t$ . Also shown are curves depicting an  $A_t^{1/3}$  and  $A_t$  dependence for comparison with the data. (b) Relative fast charged-particle yields versus target mass, referenced to the fast  $\alpha$ -particle production, for the 75-MeV  ${}^{197}\text{Au}$  bombardment.

In these optimum  $Q$ -value calculations, the Coulomb and centrifugal potentials were calculated at a classical grazing radius<sup>47</sup> for the entrance channel. At these values of the interaction radius, the nuclear potential (e.g., in a Woods-Saxon form) is small compared to other terms, and so its change during the reaction was neglected, in order to simplify the calculation. The experimental results are supported very well by this semiclassical calculation, which along with the  $A_t^{1/3}$  dependence of the total singles yields, suggests strongly that the observed fragments are produced mainly by grazing interactions which preserve continuous orbits. It should be noted, however, that the dissociation of  ${}^6\text{Li}$  into  $\alpha + d$  would produce deuterons and  $\alpha$  particles at energies very near the beam velocity, because of the low  $\alpha + d$  cluster binding (1.47 MeV). Thus both semiclassical fragment transfer and projectile breakup can account for the  $\alpha$  and deuteron energies observed. On the other hand, in the case of  ${}^3\text{He}$  and  $t$  production, the  ${}^6\text{Li} \rightarrow {}^3\text{He} + t$  separation energy is nearly 16 MeV. Since the  ${}^3\text{He}$  and  $t$  spectra do not reflect energy losses of this magnitude but instead are consistent with the optimum  $Q$  values calculated for cluster transfer, the implication is that these particles are produced primarily individually by conventional cluster-transfer processes.

The dominance of the singles spectra by  $\alpha$  and  $d$  production (with the  ${}^3\text{He}$  and  $t$  intensities ap-

proximately an order of magnitude lower) might at first suggest dominance of the  ${}^6\text{Li}$  ground-state wave function by the  $\alpha + d$  cluster structure. However, recent results from cluster knockout reactions<sup>15,16</sup> show that the  $\alpha + d$  and  ${}^3\text{He} + t$  cluster amplitudes in the  ${}^6\text{Li}$  ground state are equal in magnitude to within a factor of 2. In addition, it is also known<sup>15</sup> that the  $\alpha + d$  form factor  $|\phi_{\alpha d}(q=0)|^2$  is a factor of 10 larger than the corresponding  ${}^3\text{He} + t$  form factor  $|\phi_{{}^3\text{He}t}(q=0)|^2$ , because of the larger binding energy of the latter  ${}^6\text{Li}$  cluster configuration.<sup>48</sup> It is important to realize that quasielastic knockout yields of  ${}^6\text{Li}$  fragments depend not only on the relative percentage of the two types of  ${}^6\text{Li}$  ground-state cluster structures, but also on the magnitude of the cluster structure form factors under the conditions of low momentum transfer. Thus, it is tempting to speculate that the fragment production processes we observe in the present measurements also probe directly these cluster momentum distributions and may therefore primarily involve quasifree  ${}^6\text{Li}$  dissociation or fragment transfer.

In the singles spectra we see fast protons which are concentrated at energies which are generally higher than the beam-velocity value (12.5 MeV) and which show up as bumps superimposed on the evaporation and pre-equilibrium energy spectra from the low-mass targets. In the spectra from the  ${}^{197}\text{Au}$  bombardments, these fast protons dom-

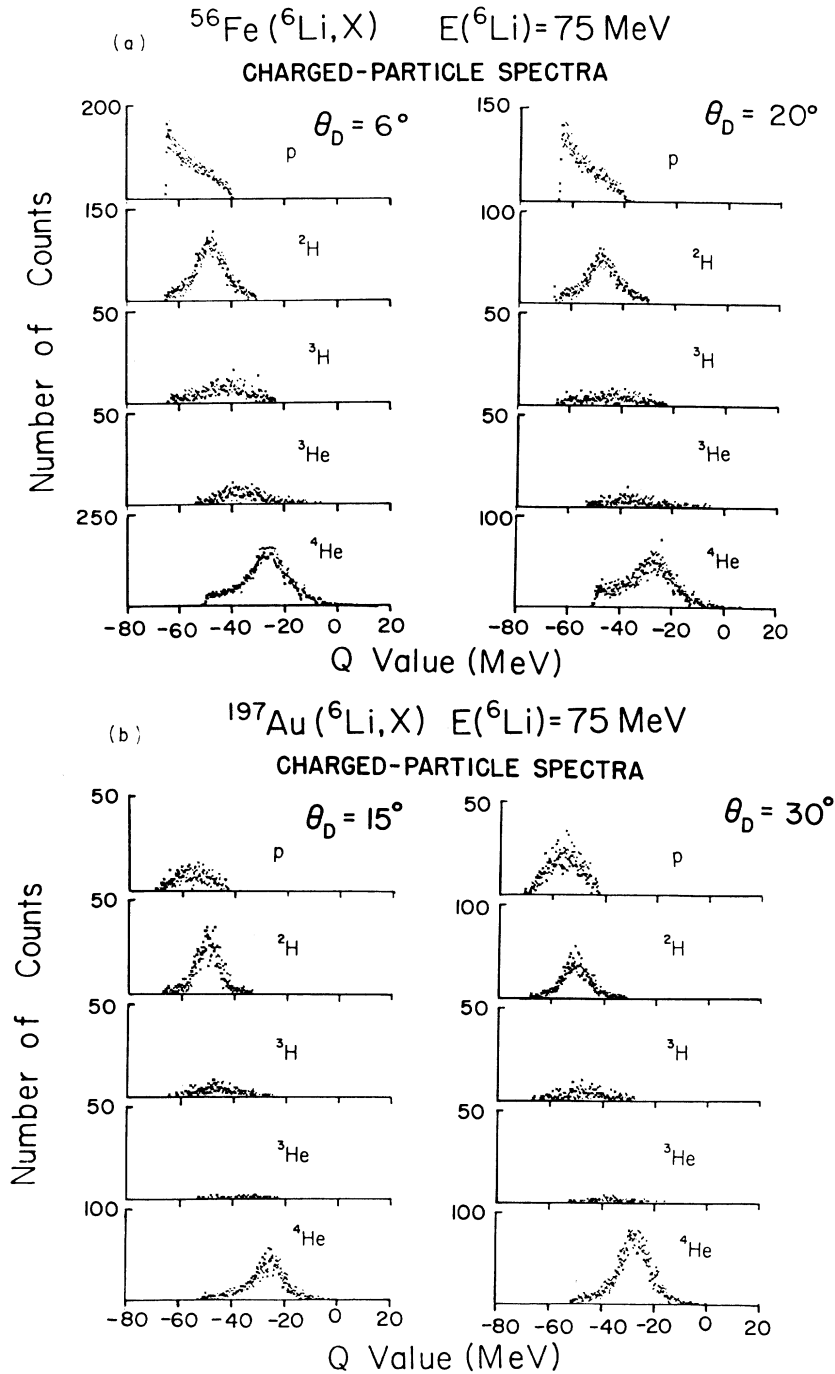


FIG. 5. Charged-particle singles spectra, plotted as a function of  $Q_k$ , defined as the  $Q$  value of the appropriate multinucleon transfer reaction which produces particle  $k$  with a lab kinetic energy  $E_k^{\text{lab}}$  [See Eq. (3) and explanatory text.] (a) Spectra of particles observed at  $\theta(\text{lab}) = 6^\circ$  and  $20^\circ$  for a  $^{56}\text{Fe}$  target and (b) at  $15^\circ$  and  $30^\circ$  for a  $^{197}\text{Au}$  target.

inate the proton spectrum and are centered at about 17 MeV (see Fig. 1). It is also interesting to note that these protons exhibit a rather flat angular distribution, with the differential production cross section ranging from 100–200 mb/sr in the angular range  $\theta_p \lesssim 50^\circ$  (see Fig. 2). For

comparison, we note that the measured differential yield of evaporation protons with this target at this beam energy is approximately 8 mb/sr,<sup>49</sup> so the observed proton flux is in fact dominated by production from nonfusion processes. These fast protons are produced with a significantly

higher (i.e., less negative) peak  $Q$  value than predicted for semiclassical 5-nucleon transfer, which tends to rule out this mechanism for their production. Relevant mechanisms for the production of protons will be discussed further when the particle correlation data are presented.

Regardless of the mechanisms of proton production, the observed flatness of the proton angular distribution can be qualitatively understood since the effective mean free path of a heavy cluster in the nucleus is considerably shorter than that of a proton.<sup>50</sup> Thus, one might expect the protons produced at low impact parameter to survive more readily than any other particle considered and thereby appear in greater numbers in the back angles.

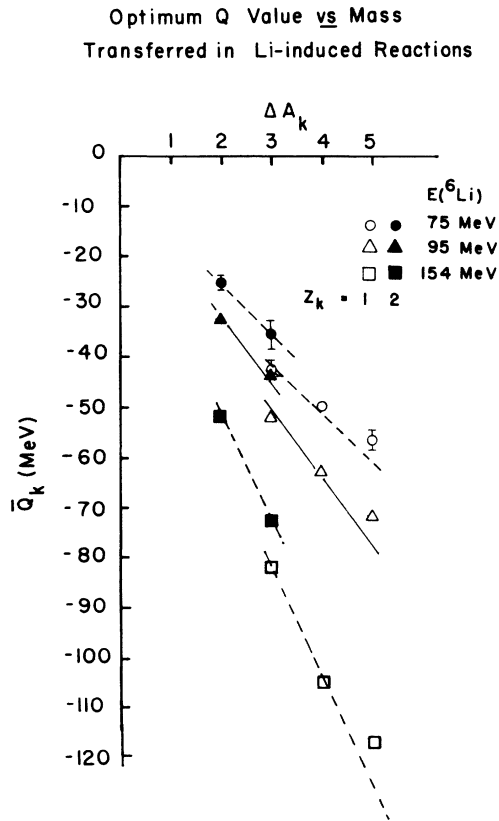
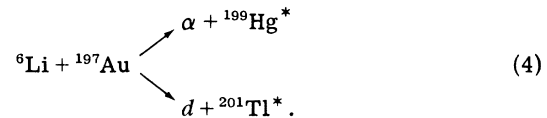


FIG. 6. Observed peak  $Q$  value for production of charged particles of type  $k$  as a function of the mass  $\Delta A_k$  transferred to the residual system. The mass of the observed particle  $k$  is therefore  $6 - \Delta A_k$  and the transferred charge is  $3 - Z_k$ . Data are shown for the present 75-MeV bombardments of  $^{197}\text{Au}$  and also for 95- and 154-MeV bombardments (Ref. 46) of  $^{197}\text{Au}$  by Vigdor and co-workers. The dashed curves are the theoretical values of the optimum  $Q$  value for the transfer of  $\Delta A_k$  nucleons, using the semiclassical formalism of Von Oertzen (Ref. 45).

### B. Particle $\gamma$ -ray coincidences

These measurements were performed specifically to determine the extent to which, as suggested by several authors,<sup>34,36-38</sup>  $^6\text{Li}$ -induced reactions proceed by the transfer of a projectile cluster to the target, followed by the decay of the residual system in the manner of a (cluster,  $xn\gamma$ ) reaction. Measurements were made of the spectra of  $\gamma$  rays in prompt coincidence with the intense beam-velocity  $\alpha$  and deuteron fluxes from the 75-MeV  $^6\text{Li}$  bombardment of  $^{197}\text{Au}$ . Results from these particular measurements have already been reported,<sup>41</sup> and the discussion given here summarizes those results.

Shown in Fig. 7 are the spectra of  $\gamma$  rays in prompt coincidence with beam-velocity  $\alpha$  particles and deuterons in this reaction. The  $\alpha$ -gated spectrum shows a clear dominance by known<sup>51</sup> transitions in  $^{196}\text{Hg}$ , and lines from the adjacent Hg isotopes are also recognized. In the deuteron-gated spectrum,  $^{197}\text{Tl}$  lines<sup>35,52</sup> predominate. The most plausible reaction mechanism which would produce these spectra involves the  $Q$ -optimum transfer of an  $\alpha$  or deuteron to the target nucleus as previously discussed. Such a reaction might be described by



The residual  $^{199}\text{Hg}^*$  or  $^{201}\text{Tl}^*$  systems thus formed decay in part by the emission of neutrons and  $\gamma$  radiation resembling that from a (fragment,  $xn\gamma$ ) reaction. As described in Ref. 41, a number of features of the particle- $\gamma$ -ray coincidence data support strongly the existence of such a reaction channel:

(a) The dominance of  $^{196}\text{Hg}$  lines in the  $\alpha$ -gated  $\gamma$ -ray spectra and of  $^{197}\text{Tl}$  lines in the  $d$ -gated  $\gamma$ -ray spectra in the 75-MeV  $^6\text{Li}$  bombardment are consistent with the known dominance by ( $d, 3n$ ) (Ref. 53) and ( $\alpha, 4n$ ) (Ref. 54) reactions at 25 and 50 MeV, respectively.

(b) The relative yields of  $^{195,196,197}\text{Hg}$  isotopes in coincidence with various  $\alpha$ -particle energy bins follows very closely the measured ( $d, 2n$ ),<sup>56</sup> ( $d, 3n$ ),<sup>54</sup> and ( $d, 4n$ ) (Ref. 57) excitation functions.

(c) The  $\alpha$ -gated  $^{196}\text{Hg}$  cascade  $\gamma$  rays exhibit a relative intensity pattern very similar to that observed in ( $d, 3n$ ) studies<sup>55</sup> on  $^{197}\text{Au}$ .

The total cross section for the production of  $\alpha$  particles at  $25^\circ$  in coincidence with  $\gamma$  rays (all of which were transitions in Hg isotopes) is  $d\sigma_{\alpha\gamma}/d\Omega_\alpha = 72 \pm 15$  mb/sr. This result was obtained from the measured coincidence cross section  $d^2\sigma_{\alpha\gamma}/d\Omega_\alpha d\Omega_\gamma$  by assuming an isotropic distribution of

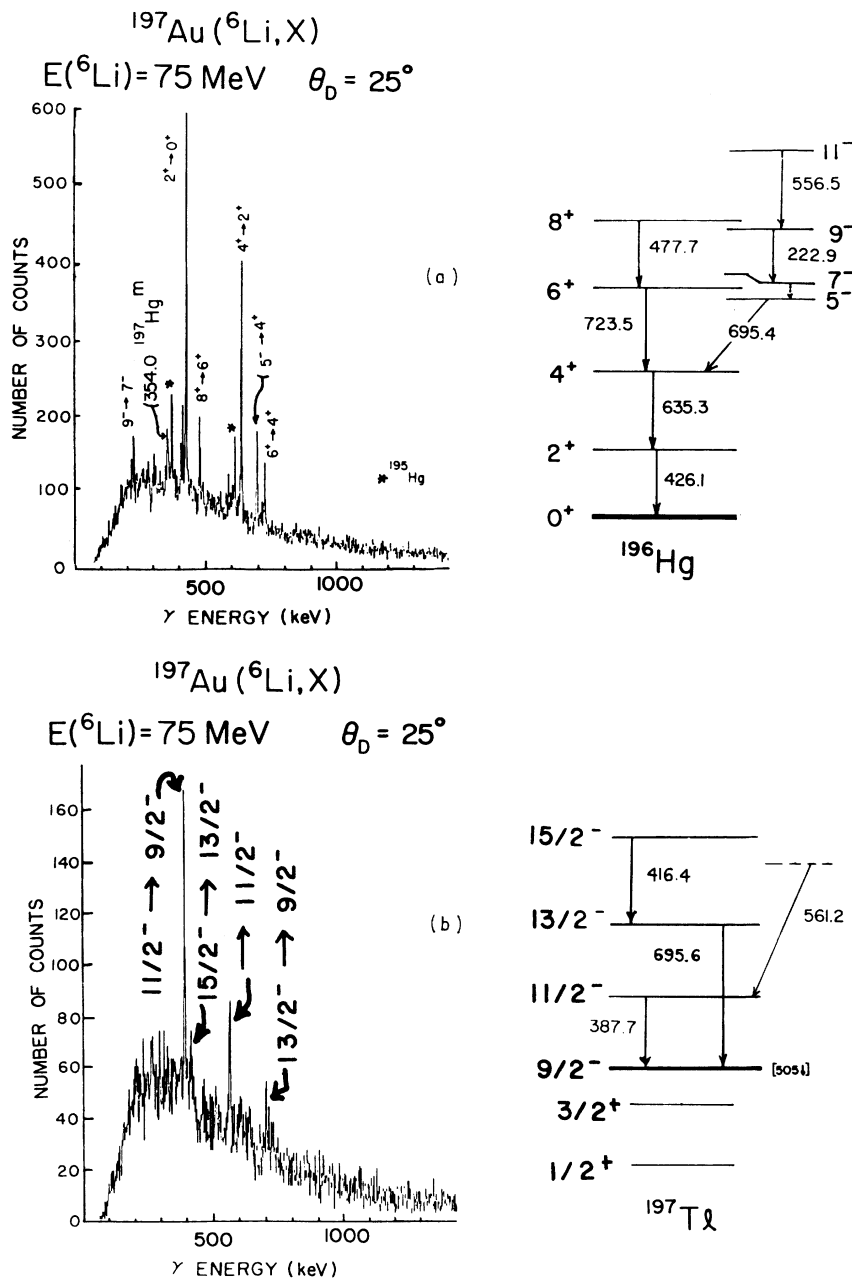


FIG. 7. Spectrum of  $\gamma$  rays in prompt coincidence with (a) beam-velocity  $\alpha$  particles and (b) beam-velocity deuterons, from the 75-MeV  $^6\text{Li}$  bombardment of  $^{197}\text{Au}$ . Insets to figures identify the transitions observed.

the coincidence  $\gamma$  rays in the laboratory. Strictly speaking, this assumption is not valid, but, as will be discussed below, the effect of expected  $\gamma$ -ray anisotropies on the accuracy of the cross section quoted above is not particularly important.

In the case of the fragment transfer reactions discussed in the present work, the axes of the charged-particle detector and the accelerator beam define a reaction plane, and in a semiclassical picture, the transferred fragments would

tend to be captured into orbits which are concentrated near this reaction plane. As a result, gamma radiation from these captures (i.e., in coincidence with the detected charged particles) would come from a polarized ensemble of nuclear states whose angular momentum vectors are oriented predominantly perpendicular to this reaction plane. This axially-symmetric polarization would give rise to uniform  $\gamma$ -ray intensity in the reaction plane; but pronounced  $\gamma$ -ray aniso-

otropies would be present out of the reaction plane. The angular distribution of quadrupole  $\gamma$  radiation from such a polarized system can be easily calculated if the relative populations of the  $m$  substates of the system are specified.<sup>58,59</sup> It can be shown that, even for the most extreme polarization of the residual system, the above integrated result for the total  $\alpha$ - $\gamma$  coincidence yield at  $\theta_\alpha = 25^\circ$  under the assumption of  $\gamma$ -ray isotropy in the lab amounts to, at most, a 20% overestimate of the particle- $\gamma$  yield, relative to the correct, angular-distribution-weighted integrated yield. It should be remarked that careful measurements of the  $\gamma$ -ray angular distribution would shed a great deal of light on the geometric features of the fragment capture process since the distribution relative to the plane of the fragment capture is so readily predictable.

For  $\gamma$  rays in coincidence with beam-velocity deuterons at  $25^\circ$  ( $^{197}\text{Tl}$   $\gamma$ -rays), the integrated cross section is  $d\sigma_{\alpha\gamma}/d\Omega_d = 15 \pm 3$  mb/sr, which is approximately 8% of the cross section with which the beam-velocity deuterons are produced in singles at  $25^\circ$ . This latter cross section is no doubt a slight underestimate, since low-energy ( $E_\gamma < 100$  keV)  $\gamma$  rays were not detected, due to the placement of a Cd absorber on the front face of the Ge(Li) detector to attenuate the intense x-ray counting rate. Thus, low-energy  $\gamma$  rays from the adjacent, odd-odd  $^{196,198}\text{Tl}$  nuclei would not have been included in the coincidence intensity.

### C. Particle-particle coincidences

Since only about 10 to 15% of the beam-velocity fragment flux can be attributed to reactions involving the transfer of one of the fragments to the target nucleus, this leads to the search for further cross sections in channels which produce *correlated* charged particles, at least one of which is a beam-velocity fragment.

Most of the possible reaction mechanisms mentioned in the Introduction give rise to production of such correlated particles, and this section deals with our in-plane particle-particle correlation measurements with which we have sought to ascertain the extent to which various mechanisms play a role in  $^6\text{Li}$ -induced reactions.

#### 1. Alpha-deuteron coincidences

Shown in Fig. 8 is the measured  $\alpha$ - $d$  angular correlation resulting from the 75-MeV  $^6\text{Li}$  bombardment of  $^{197}\text{Au}$ . Correlations are shown for the cases where the  $\alpha$ -particle detector is held fixed (black dots) and where the deuteron detector is held fixed (open circles). Both correlations were taken simultaneously and sorted

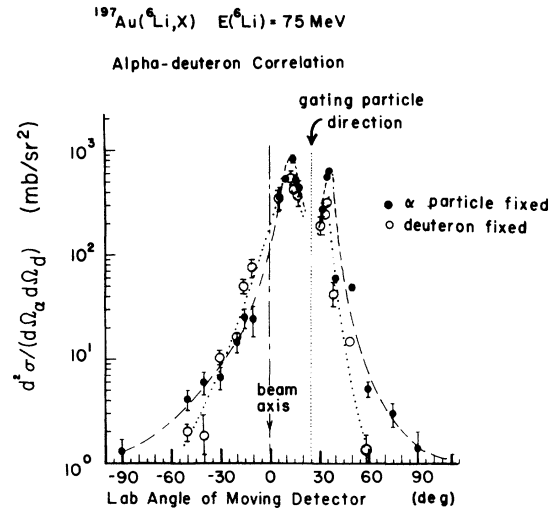


FIG. 8. Angular correlation of  $\alpha$  particles and deuterons from the 75-MeV  $^6\text{Li}$  bombardment of  $^{197}\text{Au}$ . The darkened circles represent the correlation pattern observed when the  $\alpha$ -particle detector was held fixed at  $25^\circ$  in the lab and the deuteron detector angle was varied ( $\alpha$ -gated correlation). The open circles correspond to the correlation obtained with the deuteron ( $d$ -gated correlation). For purposes of orientation, the angular positions of the beam axis and fixed detector are also indicated.

later in the off-line analysis. In both cases the fixed detector was positioned at  $25^\circ$  (lab). As will be shown by the results to follow, in the angular range,  $|\theta_{\alpha d}| \equiv |\theta_\alpha - \theta_d| \leq 13^\circ$ , the coincidence events are dominated by those from the well-known sequential breakup of the projectile excited to its 2.18-MeV  $3^+$  state. This state, whose mean life is approximately  $10^{-20}$  sec, then decays with a positive 0.71-MeV  $Q$  value to a free  $\alpha$  particle and deuteron. A velocity vector diagram of the breakup is shown in Fig. 9. In view of the relatively long lifetime of the excited  $^6\text{Li}$  compared with typical projectile transit times (the latter being on the order of  $3 \times 10^{-22}$  sec), one expects very little final-state interaction between the cluster fragments and the target nucleus. The breakup can be thought of as arising from a free, inelastically-scattered  $^6\text{Li}$ , where an internal excitation has been imparted to the projectile. From the velocity vector diagram, one can see that, for a given detector angular separation, only those correlated fragments which are emitted into specific solid angles in the  $^6\text{Li}$  center of mass are detected. In one case (the solid lines in Fig. 9) a high-energy  $\alpha$  particle and a low-energy deuteron are produced with velocities in the proper directions to admit them to the detector solid angles. In a second case (the dotted lines in Fig. 9) a slightly different direction of travel for the

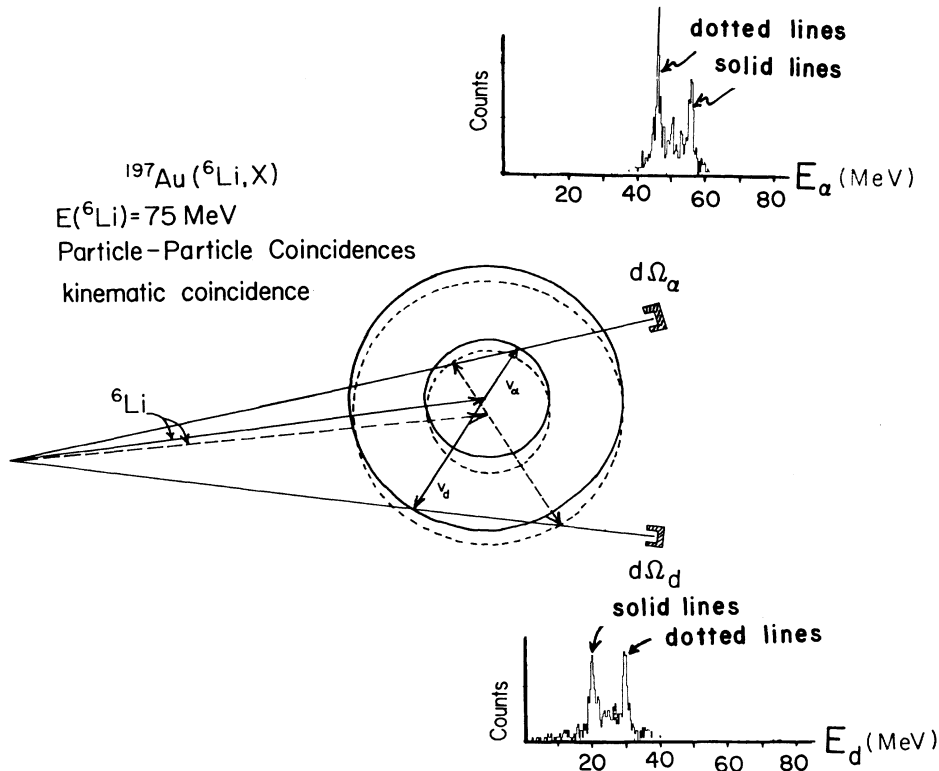


FIG. 9. Velocity vector diagram for the positive- $Q$ -value dissociation of  ${}^6\text{Li}$  into  $\alpha + d$ . The magnitude of the fragment velocity vectors in the  ${}^6\text{Li}$  center of mass are greatly exaggerated in order to depict the geometrical relationships clearly. For a given detector separation in the lab, there are two directions of velocity of the scattered  ${}^6\text{Li}$  for which the breakup fragments can be detected simultaneously. These two cases are represented by the solid and dotted lines and the resulting dual-peaked spectrum for each particle is shown in the inset near its detector. In an experimental spectrum both types of particles would be registered in each detector, resulting in four sharp peaks (see text and Fig. 10).

scattering Li projectile allows a *lower*-energy  $\alpha$  particle to be detected in coincidence with a *higher*-energy deuteron. (See insets in Fig. 9.) Reversing the roles of the two detectors results in the detection of two deuteron peaks in the upper detector and two  $\alpha$ -particle peaks in the lower detector, thus giving four sharp peaks in each detector. In the inset of Fig. 10(a) is shown a general coincidence spectrum of all correlated charged particles incident on one of the two detector telescopes for a detector separation of  $9^\circ$ . The dual peaking feature described above is clearly observed. The coincidence relationships among the  $\alpha$  particles and deuterons are shown in Fig. 10(a), where it is clear that the higher-energy  $\alpha$ -particle group is in coincidence with the lower-energy deuteron group and *vice versa*. It is evident from Fig. 9 that there should be a maximum detector angular separation, beyond which no sequential-breakup events can be detected. For 75-MeV  ${}^6\text{Li}$  breakup from the  $3^+$  state, this maximum angle is  $11.9^\circ$ . In Fig.

10(b) it can be seen that as the detector angular separation increases, the energy differences between the two  $\alpha$ -particle peaks and between the two deuteron peaks decrease; furthermore, the distinctive feature of dual pairs of peaks survives only until the detector separation reaches approximately  $13^\circ$ . One expects this critical separation to be larger than the maximum fragment separation angle because each detector subtended an angle of approximately  $1^\circ$ . Beyond this point, the  $\alpha$ - $d$  coincidence rate is very low and consists of coincidences between  $\alpha$  particles and deuterons whose energy spectra more closely resemble the singles data.

The magnitudes of these energy separations and their dependence upon  $\theta_{\alpha d}$  are in excellent agreement with the results expected from the kinematics of sequential breakup from the first excited  $3^+$  state in  ${}^6\text{Li}$ . Extensive discussions of these well-known kinematic features can be found in Refs. 60 and 61.

It is important to point out that the pronounced

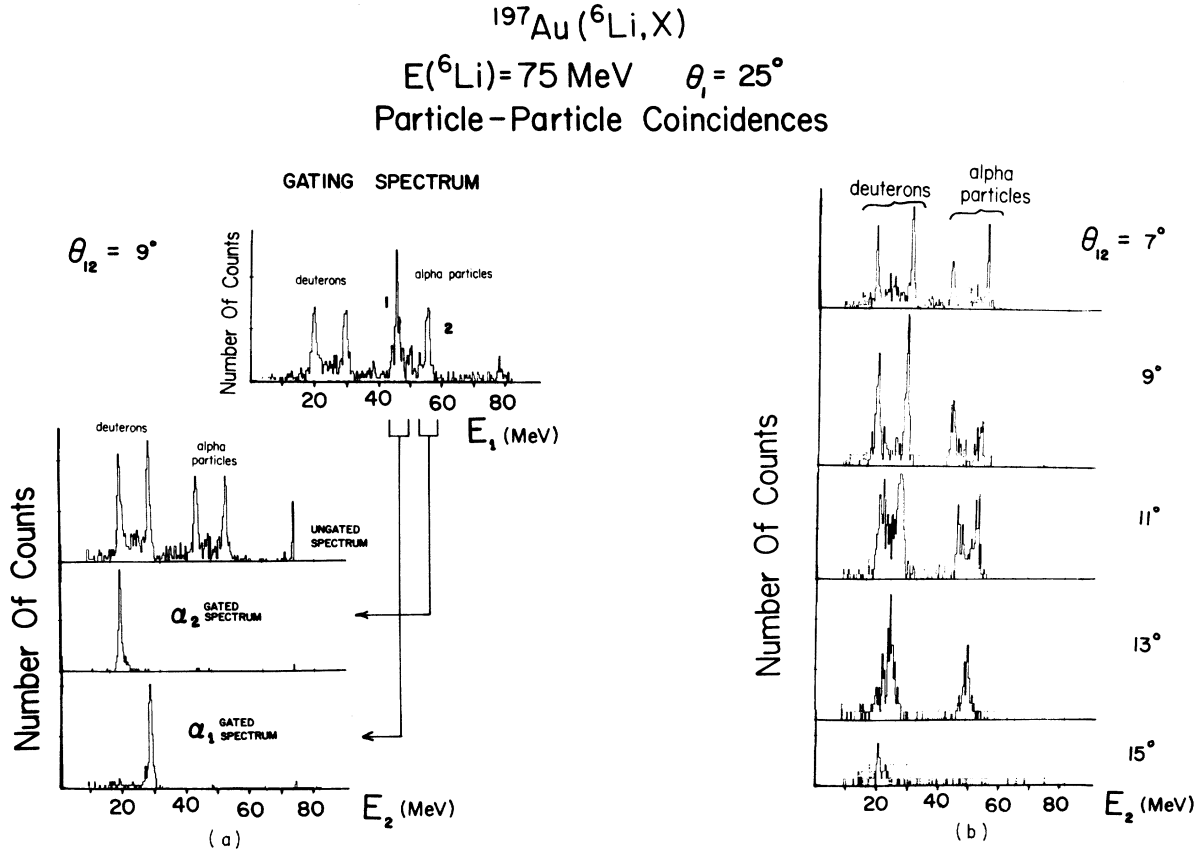


FIG. 10. (a) Schematic of the coincidence relationship between pairs of peaks in the particle-particle correlation spectra for detector angular separation less than  $13^\circ$ . The  $\alpha$ -particle peaks in detector number 1 are in coincidence with specific deuteron peaks in detector number 2, as shown in the figure. In addition, the deuteron peaks in detector number 1 are in coincidence with the  $\alpha$ -particle peaks in detector number 2 (the latter coincidence relationship not shown). (b) Depiction of the appearance of the charged-particle coincidence energy spectra as the detector angular separation is changed, showing that the dual-peaking feature survives only up to  $\theta_{ad} \approx 13^\circ$ , and that the energy separations of the two deuteron and of the two  $\alpha$ -particle peaks decrease as  $\theta_{ad}$  increases, as expected from the sequential-breakup kinematics.

double peaking in the  $\alpha$ - $d$  correlation patterns (see Fig. 8) is also a natural consequence of the kinematics of the sequential-breakup process. As pointed out by Scholz *et al.*,<sup>61</sup> for a given direction of the decaying  $^6\text{Li}$ , progressively larger solid angles in the  $^6\text{Li}$  center-of-mass system are viewed by the detectors as their angular separation increases. Thus, if isotropic  $\alpha + d$  fragment distributions in the  $^6\text{Li}$  center of mass are assumed, the coincidence counting rate will increase with  $\theta_{ad}$  until the boundary of the kinematic cone is reached. This solid angle effect accounts for the major part of the observed rise in the  $\alpha + d$  correlation as  $\theta_{ad}$  increases to approximately  $13^\circ$ .

In the above sequential-breakup picture, a given angular separation of the detectors corresponds to observation of breakup fragments which have been emitted in the  $^6\text{Li}$  center of mass so

that the deuteron emerges at a specific angle  $\theta_c$  with respect to the  $^6\text{Li}$  center-of-mass velocity (cf. Fig. 9 and Refs. 60, 61). Furthermore, a given lab direction and kinetic energy for the deuteron and for the correlated  $\alpha$  particle uniquely determine the direction of the velocity of the decaying  $^6\text{Li}$  which produced those fragments. Shown in Fig. 11 is the measured angular distribution of the  $\alpha + d$  sequential coincidence rate as a function of the effective  $^6\text{Li}$  direction in the lab,  $\theta_{L1}$ . The data points were selected for a narrow range of detector angular separations which correspond to the emission of deuterons over a restricted  $^6\text{Li}^*$  center-of-mass angular range:  $\theta_c = 60 \pm 3^\circ$  (see inset of Fig. 11). The finite solid angle subtended by the two detectors requires that the detected  $\alpha + d$  sequential-breakup coincidence events at a given detector angular separation (and therefore a given  $\theta_c$ ) correspond

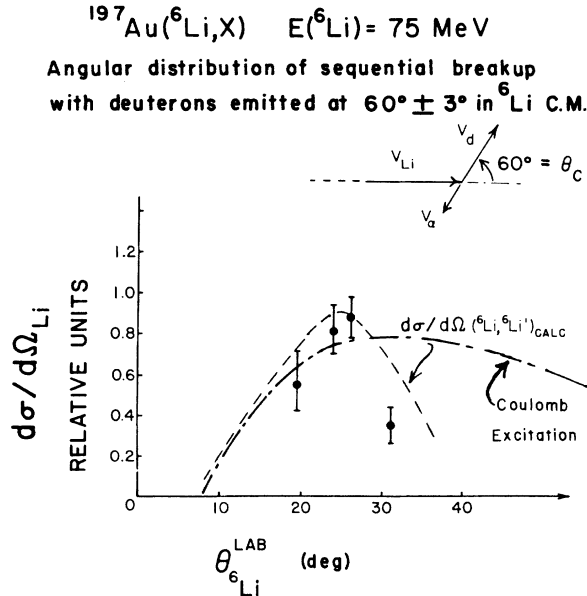


FIG. 11. Angular distribution of sequential  $^6\text{Li}$  breakup strength as a function of the effective scattering angle of the decaying  $^6\text{Li}$ . Also shown are angular distributions calculated for pure Coulomb excitation of the 2.18-MeV  $3^+$  state in  $^6\text{Li}$  and also the DWBA result (using both Coulomb and nuclear potentials) for the inelastic scattering of  $^6\text{Li}$  by excitation to its  $3^+$  state. See text for further explanation of symbols.

to dissociating  $^6\text{Li}$  nuclei scattered into a finite solid angle of magnitude  $d\Omega_{\text{Li}}$ . However, since  $|d\Omega_{\text{Li}}|$  depends only upon  $\theta_c$ , its value is essentially constant for all of the data points shown in Fig. 11. Thus the cross sections are expressed in relative units but still properly reflect the shape of the angular distribution. For comparison, we show in Fig. 11 the calculated angular distribution of inelastic scattering of  $^6\text{Li}$  by a  $^{197}\text{Au}$  target, with the outgoing  $^6\text{Li}$  projectile in its first excited state. The calculation was performed with the distorted-wave Born approximation (DWBA) method,<sup>62</sup> using a deformed form factor. Both Coulomb and nuclear excitations were included, and the spin-orbit interaction was ignored. The parameters of the optical potential were those obtained by fitting the measured  $^6\text{Li}$  elastic scattering angular distribution and were found to be similar in value to those obtained by Huffman *et al.*<sup>63</sup> from 75-MeV  $^6\text{Li}$  elastic scattering on  $^{90}\text{Zr}$ . The very close similarity between the shapes of the calculated and observed angular distributions lends credence to the increased importance of nuclear excitations, especially at low impact parameters. By contrast, the Coulomb excitation alone (also shown in Fig. 11)<sup>64</sup> cannot explain the data.

It is clear from Fig. 8 that significant  $\alpha + d$

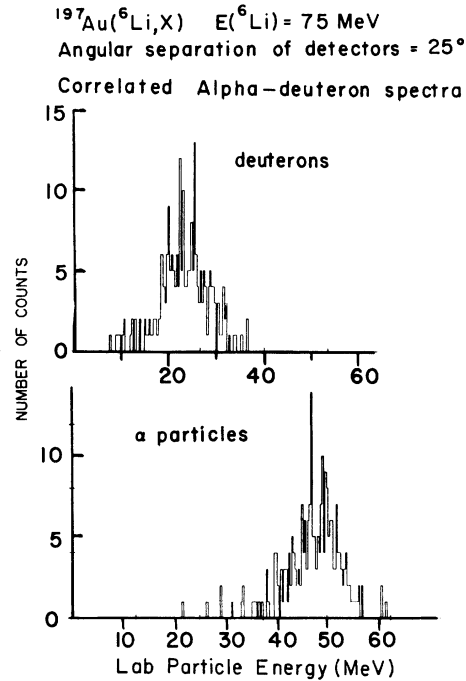


FIG. 12. Typical energy spectra of correlated  $\alpha$  particles and deuterons detected outside the kinematic cone for sequential  $^6\text{Li}$  breakup from the 75-MeV bombardment of  $^{197}\text{Au}$ .

coincidence cross section exists beyond the sequential-breakup kinematic cone. The  $\alpha$  and  $d$  energy spectra in the coincidence events outside this cone (an example of which is shown in Fig. 12) do not exhibit any discernible structure, but instead are grouped in a broad peak near beam-velocity energies. These coincidences may be the result of a direct, quasifree breakup process in which the  $\alpha$  particle and deuteron are liberated by sudden interaction of the loosely bound  $^6\text{Li}$  with the target nuclear field. Furthermore, one might then anticipate that the observed spread in the energy distribution of the outgoing fragments is simply a reflection of the momentum distribution of the clusters in the  $^6\text{Li}$ . This concept was explored by Serber<sup>65</sup> with regard to the neutron energy spectrum from the breakup of the deuteron. Some applications of this idea have also been made in heavy-ion reactions<sup>1,66</sup> and recently in the study of  $\alpha$ -particle breakup.<sup>67</sup>

An interesting feature of the  $\alpha + d$  correlation (cf. Fig. 8) is that, for a fixed  $\alpha$ -particle direction, there appear to be more correlated deuterons toward the beam direction than away from it. The same features are noticed with respect to  $\alpha$  particles in the  $d$ -gated correlation (cf. Fig. 8, open circles). The detector solid angle effect discussed above<sup>61</sup> will produce a *symmetric*, double-humped angular correlation of sequential-

breakup events for a given lab direction of the scattered  ${}^6\text{Li}^*$ , assuming isotropy of the  $d$  and  $\alpha$  angular distributions in the  ${}^6\text{Li}^*$  center-of-mass system. The  $\alpha + d$  correlation data taken here correspond to  ${}^6\text{Li}^*$  scattering angles distributed symmetrically about  $25^\circ$  (lab). Since the  ${}^6\text{Li}^*$  angular distribution (discussed above and shown in Fig. 11) peaks at approximately  $25^\circ$ , one might expect relatively little asymmetry due to the  ${}^6\text{Li}$  scattering. However, the  $\alpha + d$  center-of-mass isotropy assumption may be open to some question,<sup>23,61,68</sup> so one cannot rule this out as a possible contributor to the  $\alpha + d$  correlation asymmetry observed.

In Fig. 13 are presented correlated  $\alpha - d$  energy spectra from two of the coincidence runs. The events in Fig. 13(a) were acquired within the sequential-breakup cone and are therefore dominated by the dual-peaking feature described above. The events in Fig. 13(b) were outside the sequen-

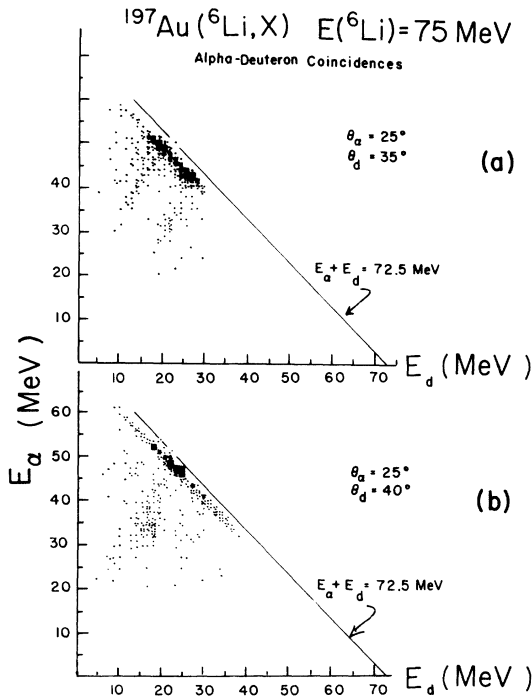


FIG. 13. Correlated energy spectra for the  $\alpha - d$  coincidence measurements from the 75-MeV  ${}^6\text{Li}$  bombardment of  ${}^{197}\text{Au}$ . In part (a) the coincidence events are detected within the sequential-breakup cone, and in (b) the events are just outside the limits of this cone. It should be noted that these plots are a result of the gating of  $\alpha$  particles in one detector and deuterons in the other. The complementary set of  $\alpha - d$  coincidences, obtained by interchanging the type of particle gated in each detector, would appear in the lower right-hand portions of the figures. This latter type of coincidence has been suppressed in the plots for the sake of clarity.

tial-breakup cone, and the particle energies are clearly grouped around the beam velocity as in Fig. 12. In a simple picture of the  ${}^6\text{Li}$   $\alpha + d$  dissociation (regardless of the mechanism), the kinetic energies of the correlated  $\alpha$  particle and deuteron should equal the incident  ${}^6\text{Li}$  energy minus the  $\alpha + d$  binding energy. For a 75-MeV  ${}^6\text{Li}$  beam, this value (including assumed 0.5-MeV energy losses from the traversal of the  ${}^{197}\text{Au}$  target and from recoil of the target) will be 72.5 MeV. The locus  $E_\alpha + E_d = 72.5$  MeV is plotted in Figs. 13(a) and 13(b), and the coincidence events in both cases are definitely within this kinematic limit.

It is interesting to note that both within and just beyond the boundary of the sequential-breakup cone are highly inelastic events associated with each of the intense  $\alpha + d$  coincidence peaks. The strong inelastic group in Fig. 13(b) corresponds to an excitation range in the  ${}^{197}\text{Au}$  residual system of approximately 17 to 25 MeV.

For detector positions on opposite sides of the beam, the correlated particles are spread out over a wider range of energies, and the centroids of the particle energy distributions tend to occur at energies below the beam-velocity values.

Integration of the  $\alpha + d$  correlation over deuteron angles gives the differential cross section for the production at  $25^\circ$  (lab) of  $\alpha$ 's which are involved in the sequential and nonsequential coincidences discussed above. Without knowledge of the correlation over the entire solid angle sphere, we cannot perform this integration. However, if one makes the simplifying assumption of azimuthal symmetry of the correlation about the axis defined by the lab direction of the gating  $\alpha$  particle (see below), then the angular integration of the correlation gives the result  $d\sigma_{\alpha d}/d\Omega_\alpha = 143 \pm 22$  mb/sr at  $\theta_\alpha = 25^\circ$ . This result accounts for approximately 25% of the singles fast  $\alpha$ -particle production cross section at this angle ( $570 \pm 62$  mb/sr, cf. Fig. 2). Integration of the  $\alpha$ -gated correlation within the sequential-breakup cone ( $\theta_{\alpha d} \leq 13^\circ$ ), under the same simplifying symmetry assumption used above, gives the result  $d\sigma_{\alpha d}/d\Omega_\alpha = 70 \pm 10$  mb/sr for  $\alpha$  particles into  $25^\circ$  which arise primarily from the sequential-breakup process.

The above azimuthal symmetry assumption is somewhat *ad hoc*, used in order to achieve a manageable quantitative estimate of the integrated cross section from the limited data available. If the angular distributions in the  ${}^6\text{Li}^*$  center of mass of the *individual*  $\alpha$  and  $d$  fragments from sequential decay are isotropic (as is generally believed), then this assumption is reasonable, undermined only by the forward-peaked aniso-

trophy of the  ${}^6\text{Li}^*$  particles over the angular range covered in the  $\alpha + d$  correlation. Furthermore, this  ${}^6\text{Li}^*$  anisotropy effect is averaged out to some extent by an angular integration which relies upon isotropy. It is also true that polarization effects in the  ${}^6\text{Li}$  inelastic scattering should not affect the validity of this assumption, since the fragment isotropy in the  ${}^6\text{Li}^*$  center of mass removes the relevance of the orientation of the  ${}^6\text{Li}^*$  angular momentum vector. (It should be noted that there is some evidence for slight anisotropy of the  $\alpha$  and  $d$  fragments in the  ${}^6\text{Li}^*$  center of mass,<sup>61</sup> so the integrated cross sections quoted above should be taken only as estimates, carrying more than just statistical uncertainty. Furthermore, it is not at all obvious that the azimuthal symmetry assumption would be as valid for *all* of the  $\alpha + d$  coincidence production mechanisms discussed here; however, we extend the assumption to include these cases as well, in order to minimize complications in arriving at estimates of the cross sections obtained by integration of the total  $\alpha + d$  correlation results.)

### 2. ${}^3\text{He}$ - $t$ coincidences

During the course of the coincidence measurements, no  ${}^3\text{He}$  or tritons were observed in any coincidence spectrum, implying that these particles were produced individually. This information and the singles energy spectra of the  ${}^3\text{He}$  and  $t$  favor the conventional ( ${}^6\text{Li}, t$ ) and ( ${}^6\text{Li}, {}^3\text{He}$ ) fragment-transfer reactions as the dominant mechanisms by which these particles are produced. These reactions would likely be enhanced at the optimum  $Q$  value as discussed earlier, and so the observed  $Q$ -value behavior of the particle spectra is also reasonable.

### 3. Alpha-proton coincidences

The  $\alpha + p$  angular correlation is shown in Fig. 14. The solid data points are for the measurements with the  $\alpha$ -particle direction fixed at  $25^\circ$  (lab) and the proton detector angle varying. The open circles correspond to data taken with the proton detector fixed at  $25^\circ$  (lab). Several features of this correlation merit emphasis: (a) Most of the coincidences are concentrated in a small angular range around the gating particle direction. (b) The correlation pattern exhibits a double-humped shape about the gating particle direction. (c) As in the case of the  $\alpha + d$  correlation, both  $\alpha + p$  correlations exhibit asymmetry about the gating particle direction. This asymmetry is especially pronounced in the  $\alpha$ -gated correlation, where the coincidence proton inten-

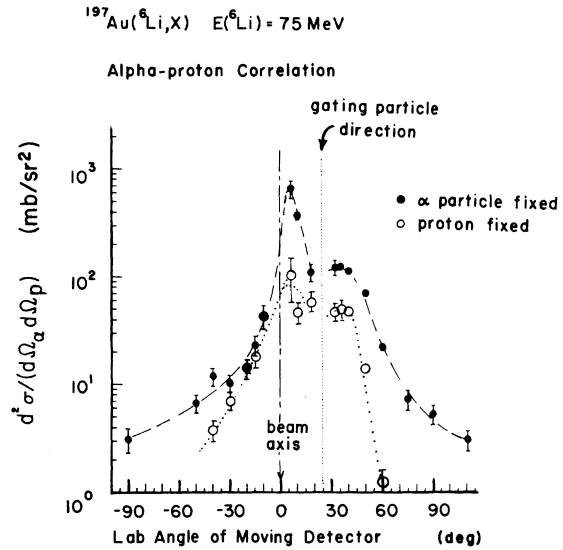


FIG. 14. Angular correlation of  $\alpha$  particles and protons for the 75-MeV  ${}^6\text{Li}$  bombardment of  ${}^{197}\text{Au}$ . The darkened circles represent the correlation pattern observed when the  $\alpha$ -particle detector was held fixed at  $25^\circ$  in the lab and the proton detector angle was varied ( $\alpha$ -gated correlation). The open circles correspond to the correlation obtained with the proton detector fixed at  $25^\circ$  and the  $\alpha$ -particle detector moving ( $p$ -gated correlation). For purposes of orientation, the angular positions of the beam axis and the fixed detector are also indicated.

sity in the hump closer to the beam direction is nearly an order of magnitude higher than in the other hump. (d) There is significant coincidence intensity extending to negative correlation angles. (e) In the proton-gated correlation, the correlated  $\alpha$ -particle intensity falls off more rapidly with increasing detector angular separation.

In Fig. 15 are a number of two-dimensional correlated  $\alpha + p$  energy spectra. In all of these measurements, there is a total correlated energy,  $E_\alpha + E_p$ , above which no coincidence events are observed. For  $\alpha$ - $p$  angular separations  $\theta_{\alpha p}$  of  $10^\circ$  and  $15^\circ$  [Figs. 15(a) and 15(b)] the coincidence events appear to be grouped into two separate bands along the  $E_\alpha$  direction, with proton energies centered at approximately 7 and 22 MeV for  $\theta_{\alpha p} = 10^\circ$  and 8 and 20 MeV for  $\theta_{\alpha p} = 15^\circ$ . For  $\theta_{\alpha p} = 25^\circ$  [Fig. 15(c)], the coincidence events occur in a single group centered roughly around  $E_p = 13$  MeV and  $E_\alpha \leq 50$  MeV.

One can imagine several possible mechanisms by which correlated  $\alpha$  particles and protons could be produced. For each of these mechanisms we can estimate an expected upper limit for  $E_\alpha + E_p$ . In the mechanisms discussed below, we assume that the lab  ${}^6\text{Li}$  kinetic energy available for reaction is 74 MeV [75 MeV (beam energy) less 0.5-

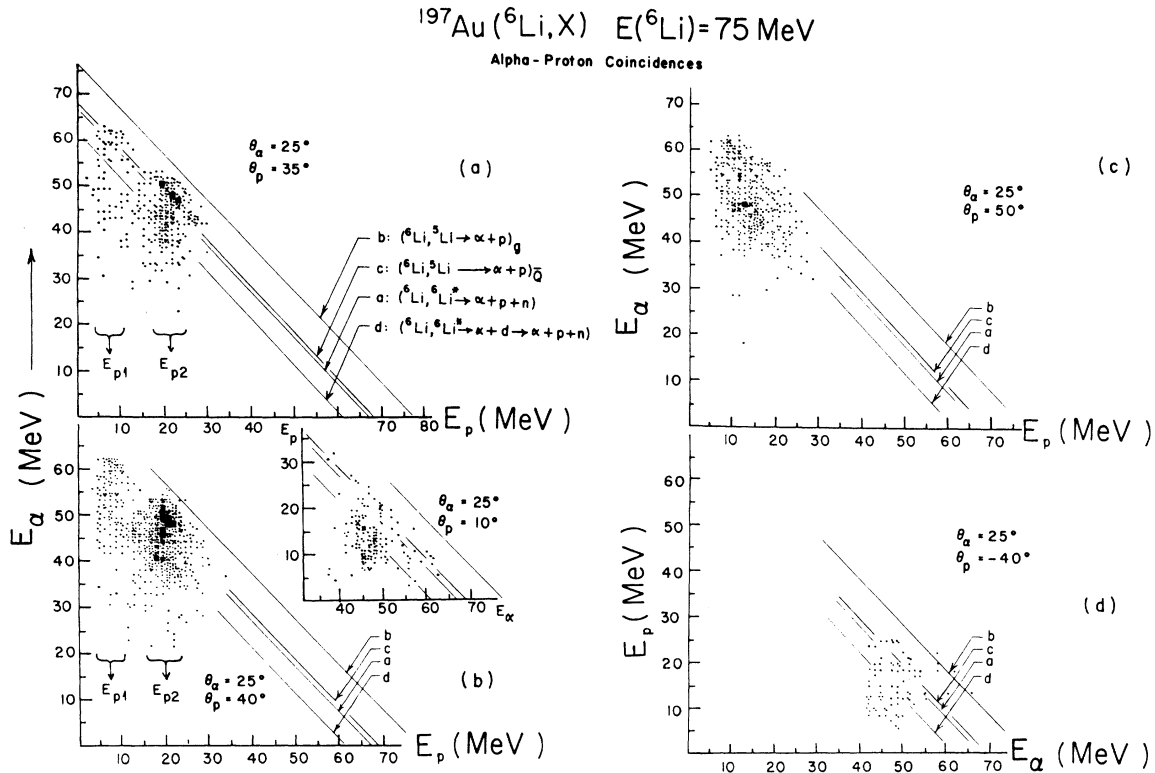


FIG. 15. Correlated energy spectra for the  $\alpha$ -proton coincidence measurements from the 75-MeV  ${}^6\text{Li}$  bombardment of  $^{197}\text{Au}$ . In all four figures the  $\alpha$ -particle detector is fixed at  $25^\circ$  in the laboratory. (a) The proton detector was placed at  $35^\circ$ , making the detector angular separation  $10^\circ$ . (b) The proton detector was set  $15^\circ$  back of the  $\alpha$ -particle detector at  $40^\circ$ . In the inset to part (b), the proton detector was located  $15^\circ$  forward of the  $\alpha$  detector. (c) The proton detector was situated  $25^\circ$  back of the  $\alpha$ -particle detector. (d) The proton detector was set on the opposite side of the beam from the  $\alpha$ -particle detector with a resulting angular separation of  $65^\circ$ . In this last correlation the roles of the two detectors have been reversed. The solid diagonal lines correspond to maximum total energies to which the correlated  $\alpha$  particle and proton energies should sum if they are produced by the reaction mechanism which labels each line. The designations of the reaction mechanism for each of the labels  $a$ - $d$  are shown in part (a) of the figure and are discussed in the text. It should be noted that these plots are a result of the gating of  $\alpha$  particles in one detector and protons in the other. The complementary set of  $\alpha$ - $p$  coincidences, obtained by interchanging the type of particle gated in each detector, would appear in the lower right-hand portions of parts (a)-(c) and in the upper-left-hand portion of part (d). This latter type of coincidence has been suppressed in the plots for the sake of clarity.

MeV energy losses from traversal of the  $^{197}\text{Au}$  target and from target recoil]:

(a) In the statistical (three-body) breakup of the excited  ${}^6\text{Li}$ , the  $\alpha + p + n$  threshold is 3.7 MeV, but the nearest states in  ${}^6\text{Li}$  from which  $\alpha + p + n$  decay could energetically occur are above 5 MeV. If one assumes excitation of the  ${}^6\text{Li}$  to its 5.37-MeV state, then a maximum value of  $E_\alpha + E_p$  of 66.7 MeV is obtained for the minimum neutron lab energy of 6 MeV. This kinematic locus is labeled  $a$  in Fig. 15. However, it is important to realize two points: (1) that this kinematic limit is computed for the *extremes* of the statistical energy distribution, implying that the bulk of the coincidence events should lie *below* this limit and none above it, which is contrary to observation; and (2) as discussed earlier,  $\alpha + p + n$  decay

has not been observed from any of the excited states of  ${}^6\text{Li}$  below 25 MeV.<sup>69</sup> Thus, this mechanism of  $\alpha + p$  production is ruled out.

(b) Neutron transfer to the ground state of  $^{198}\text{Au}$  would produce unstable  ${}^5\text{Li}$ . The  $Q$  value for this transfer is +0.87 MeV which, combined with the 1.97-MeV  ${}^5\text{Li}$  dissociation energy, gives a maximum  $E_\alpha + E_p$  of 76.8 MeV. This locus is designated as  $b$  in Fig. 15.

(c) The optimum  $Q$  value for neutron transfer to the target is  $-7.7$  MeV (calculated by the method outlined in Ref. 45). Under these conditions the maximum  $E_\alpha + E_p$  is 8.6 MeV below that of the ground-state transfer mechanism, or 68.2 MeV (locus  $c$  in Fig. 15).

(d) One might imagine the possibility of  ${}^6\text{Li}$  dissociating into an  $\alpha$  and a deuteron followed by

$p + n$  breakup of the deuteron. This mechanism results in a maximum  $E_\alpha + E_p$  value of approximately 61 MeV, plotted as locus  $d$  in Fig. 15. Since most of the coincidence intensity lies *above* this limit, this reaction mechanism is also ruled out.

The picture which emerges from the consideration of the correlated  $\alpha$ - $p$  energy spectra is that the primary reaction mechanism involves the production of  ${}^5\text{Li}$  by neutron transfer to the target. Let us consider the data further in this context. The appearance of two groups of  $\alpha$ - $p$  coincidences associated with two proton energies, for angular separations of  $10^\circ$  and  $15^\circ$  [see Figs. 15(a) and 15(b)], and their coalescence into one group for separations greater than  $24^\circ$ , the maximum  $\alpha$ - $p$  lab angular separation for the breakup of a 68-MeV  ${}^5\text{Li}$  from its ground state [cf. Fig. 15(c)], is a characteristic of sequential-breakup coincidences, which therefore supports the neutron-transfer picture in this case. One would not expect particularly sharp energy structure in the  $\alpha$ - $p$  coincidence spectra from a  ${}^5\text{Li}$  breakup, since the very short  ${}^5\text{Li}$  lifetime ( $4.4 \times 10^{-22}$  sec) would likely result in strong final-state interactions between its fragments and the target nucleus. Qualitatively speaking, we could interpret the situation in which the  $\alpha$  particles are detected forward of the protons [cf. Figs. 15(a) and 15(b)] as corresponding to the case where the  ${}^5\text{Li}$  fragment closer to the target during the interaction is the  $\alpha$  particle. Such experimental data have been similarly interpreted by Gamp *et al.*,<sup>2</sup> in heavy-ion studies. In the present case, one would then expect the final-state interactions to distort the  $\alpha$ -particle energy structure more than the protons. Thus, the observed greater spreading in energy for the  $\alpha$ 's compared with the protons as seen in Figs. 15(a) and 15(b) would seem to be consistent with this interpretation. Similarly, when the proton is detected at an angle forward of the  $\alpha$  particle, then we would expect that the *proton* energies would be more smeared out than those of the  $\alpha$  particle. Indeed, such is the case, as can be seen in the inset of Fig. 15(b) where the coincidence events appear to be more localized in  $\alpha$ -particle energy than in proton energy. Finally, the energy separation of the correlated proton groups in Figs. 15(a) and 15(b) are seen to be approximately 15 and 12 MeV for  $\theta_{\alpha p} = 10^\circ$  and  $15^\circ$ , respectively. This is in reasonable agreement with the proton energy group separations of 17 and 15 MeV calculated for  ${}^5\text{Li}$  breakup from its ground state. For the correlated energy spectrum for coincidences between particles on opposite sides of the beam [Fig. 15(d)], the particle energy distribution

centroids are approximately at the beam velocity. However, the coincidence events are widely distributed in energy, suggestive of inelasticities which one would expect from strong final-state interactions.

As in the case of the  $\alpha$ - $d$  correlation, precise determination of the differential cross section for  $\alpha$ - $p$  coincidences for  $\theta_\alpha = 25^\circ$  is not possible without complete knowledge of the correlation at all angles. However, assuming symmetry of the correlation for  $\theta_p > 25^\circ$  about the  $\alpha$ -particle direction gives the integrated result  $d\sigma_{\alpha p}/d\Omega_\alpha = 128 \pm 25$  mb/sr at  $\theta_\alpha = 25^\circ$ . This result must, of course, be regarded as a lower limit, since the full contribution of the large peak in the correlation for  $\theta_p$  between  $0^\circ$  and  $25^\circ$  was not included in the estimate. A rough upper limit to this contribution is taken as  $\frac{1}{4}$  of the symmetric integration of the peak about the  $\alpha$ -particle direction, the result of which is 57 mb/sr. Thus the quoted cross section for  $\alpha$ - $p$  correlations with  $\alpha$  particles at  $25^\circ$  is taken as  $d\sigma_{\alpha p}/d\Omega_\alpha = 156 \pm 50$  mb/sr for  $\theta_\alpha = 25^\circ$ .

#### IV. SUMMARY AND CONCLUSION

The production of fast particles with  $Z=1$  and 2 in  ${}^6\text{Li}$ -induced reactions on heavy nuclei is the result of the combined effect of several competing processes, which, as has been shown in the last section, strongly depend on the cluster structure of the projectile and which mainly occur at the surface of the target. These mechanisms are as follows:

(a) Optimum  $Q$ -value transfer of one of the possible clusters to the target. This mechanism accounts for most of the  ${}^3\text{He}$  and triton production, and a substantial portion of the alpha-particle and deuteron production.

(b) Sequential  $\alpha + d$  breakup of the  ${}^6\text{Li}$ , after it has been excited to its  $3^+$  state through the combined effect of the nuclear and Coulomb fields of the target.

(c) Nonsequential breakup of  ${}^6\text{Li}$  which occurs on a time scale comparable to the transit time of the projectile. This process was identified through the events which lie outside the kinematic cone of the sequential breakup.

(d) Optimum  $Q$ -value transfer of a neutron to the target, with the subsequent decay of the  ${}^5\text{Li}$  ground state into an alpha particle and a proton.

In order to ascertain, with the limited amount of information at hand, whether or not the reaction mechanisms discussed account for the bulk of the singles production of fast particles, Table II presents the results of the comparison of measured cross sections for each mechanism pro-

TABLE II. Summary of estimated differential cross section for fast-particle production at 25° for various reaction mechanisms and comparison with total singles yields of the same particles at 25° from the 75-MeV  ${}^6\text{Li}$  bombardment of  ${}^{197}\text{Au}$ .

Reaction mechanism	$\frac{d\sigma_{\alpha i}}{d\Omega_{\alpha}}$ (mb/sr) <sup>a</sup>	$\frac{d\sigma_{di}}{d\Omega_d}$ (mb/sr) <sup>a</sup>	$\frac{d\sigma_{pi}}{d\Omega_p}$ (mb/sr) <sup>a</sup>
$\alpha + d$ Sequential + breakup nonsequential	143 ± 22	88 ± 44 <sup>d</sup>	0
( ${}^6\text{Li}, {}^5\text{Li} \rightarrow \alpha + p$ )	156 ± 50	0	76 ± 30 <sup>e</sup>
( ${}^6\text{Li}, \alpha xn\gamma$ )	72 ± 15	0	0
( ${}^6\text{Li}, dxn\gamma$ )	0	≥ 15 ± 13	0
( ${}^6\text{Li}, pxn\gamma$ )	0	0	10 ± 2
( ${}^6\text{Li}, {}^5\text{He} \rightarrow \alpha + n$ )	(156 ± 50) <sup>b</sup>	0	0
TOTAL	371 ± 57 (527 ± 75) <sup>c</sup>	103 ± 44	86 ± 30
Measured singles yield	570 ± 62	203 ± 40	117 ± 18 <sup>f</sup>

<sup>a</sup>Differential yield of  $\alpha$  particles ( $d\sigma_{\alpha}$ ), deuterons ( $d\sigma_d$ ), and protons ( $d\sigma_p$ ) at 25° (lab) due to reaction mechanism  $i$ .

<sup>b</sup>Taken as equal to the cross section for  ${}^5\text{Li}$  production.

<sup>c</sup>Result including estimated  ${}^5\text{He}$  production.

<sup>d</sup>Estimated to be  $\frac{1}{4}$  of the result obtained by integration of the  $\alpha$ - $d$  correlation in Fig. 8 (open circles) for  $\theta_d < 25^\circ$ . An arbitrary 50% error is assigned.

<sup>e</sup>Taken as the average of the integrated  $\alpha$ - $p$  correlation in Fig. 14 (open circles) for  $\theta_p > 25^\circ$  and  $\theta_p < 25^\circ$ .

<sup>f</sup>Taken as the total singles yield less the evaporation yield of 8 mb/sr (Ref. 49).

posed with the total singles yields at 25°. In column 1 of the table are listed the differential cross sections for the production of beam-velocity  $\alpha$  particles. The individual cross sections quoted are those given in the previous sections. In addition, it should be noted that we have included the possibility that proton transfer also occurs, forming particle-unstable  ${}^5\text{He}$  which decays into  $\alpha + n$ . Since no measure of the proton transfer cross section could be made, its contribution to the fast  $\alpha$ -particle flux was assumed, for the purposes of this comparison, to be equal to that of the neutron transfer reaction; although, actual knowledge of the contributions from this process could only come from alpha-particle-neutron correlation measurements.

One should stress that this comparison does not mean the relative contributions from each of these mechanisms necessarily is the same at all angles. The quoted uncertainties in all the entries in Table II are relatively large, due to the assumptions that had to be made regarding supposed symmetries in the correlations and which could not be verified. For completeness, the differential cross sections associated with the deuteron and proton yields at 25° are also included in Table II. These cross sections were determined in the same manner as those connected with the  $\alpha$ -particle yields, and so they also contain large inherent uncertainty. Nevertheless, it can be

concluded from the table that the mechanisms proposed tend to account for all of the singles yields of protons, deuterons, and  $\alpha$  particles at 25°. It is also clear that the excess of  $\alpha$  particles seen in the singles compared with deuterons has a natural origin in the existence of reaction mechanisms which produce  $\alpha$  particles but not correlated deuterons.

A mechanism which has not been considered is deuteron pickup, leading to the formation of unstable  ${}^8\text{Be}$  which in turn decays into two  $\alpha$  particles. This process would have been impossible to observe in the present experimental setup, due to the very small opening angle between the emerging correlated  $\alpha$  particles. However, contribution from this mechanism cannot be ruled out and would, of course, add to the fast  $\alpha$ -particle yield.

Finally, some features of the observed angular correlations deserve special attention. These are as follows:

- (i) The asymmetry of the correlation with respect to the fixed particle direction ( $\theta \equiv 25^\circ$ ) amounting to a shift towards the beam direction.
- (ii) The existence of coincidence events for large angular separations  $25^\circ < \Delta\theta < 110^\circ$ .
- (iii) The faster drop in the coincidence intensities when the particle detected in the fixed direction is other than an  $\alpha$  particle.

The above features cannot be ascribed to that

component of the observed coincidence events which are due to the sequential-breakup process, since the dissociation in this case occurs too far from the nucleus to enable the final-state interactions to modify the corresponding correlation pattern. In the case of the nonsequential breakup such interactions can modify the correlations because, for a fragment detected at a particular angle, the changes in the trajectory of the second fragment depend upon its relative location (i.e., its impact parameter) in the nuclear field. Further coincidence intensities would depend not only upon the kind, but also upon the exact trajectory of the second fragment due to different absorption for different cases. For example, the shift of the correlation pattern towards the beam direction may be due to partial orbiting by the second fragment, as is expected in a semiclassical view, when its impact parameter is in the vicinity of the grazing value. For smaller values of the impact parameter, the second fragment can be anticipated to suffer large deflections towards backward directions. These effects could explain the observation of coincidence events for large separation angles on both sides of the location of the fixed detector. Similarly, the faster drop in the coincidence intensities at large angular separation (especially towards backward angles), when the second fragment is an  $\alpha$  particle, could be due to its stronger absorption when it has the smallest impact parameter or when its trajectory is longer in the nuclear field (orbiting). Whether

these ideas or any others are the bases of the special features of the correlations mentioned above must await measurements in coincidence geometries other than reported here.

In summary, our results for  ${}^6\text{Li}$ -induced reactions at super-Coulomb-barrier energies reveal, as expected, extensive participation by nuclear interactions: The Coulomb-induced sequential projectile breakup (the only breakup mode apparently present at sub-Coulomb beam energies) is supplemented by significant sequential breakup driven by nuclear excitation of the  ${}^6\text{Li}$ . Additional reaction mechanisms have also been observed to come into play, such as nonsequential  $\alpha + d$  breakup, fragment transfers, and nucleon transfer followed by fragmentation of the outgoing projectile. Finally, approximate estimates of the relative contributions of each of the mechanisms observed suggest that the bulk of the fast-particle yields can be accounted for by the observed data.

#### ACKNOWLEDGMENTS

The authors wish to express their appreciation to the IUCF operating crew for their cooperation in all of the bombardments. We would also like to thank Professor G. T. Emery, Professor S. E. Vigdor, Professor J. Jastrzebski, and Professor O. W. B. Schult for helpful discussions. This work was supported by the National Science Foundation.

\*Present address: Crocker Nuclear Laboratory, University of California, Davis, California 95616.

†Present address: Los Alamos Scientific Laboratory, MS 540, P. O. Box 1663, Los Alamos, New Mexico 87545.

‡Permanent address: INR, Swierk, near Warsaw, Poland.

<sup>1</sup>H. C. Britt and A. R. Quinton, *Phys. Rev.* **124**, 877 (1961).

<sup>2</sup>A. Gamp, J. C. Jacmart, N. Poffe, H. Doubre, J. C. Roynette, and J. Wilczynski, *Phys. Lett.* **74B**, 215 (1978).

<sup>3</sup>J. W. Harris, T. M. Cormier, D. F. Geesaman, L. L. Lee, Jr., R. L. McGrath, and J. P. Wurn, *Phys. Rev. Lett.* **38**, 1460 (1977).

<sup>4</sup>J. M. Miller, *Phys. Rev. Lett.* **40**, 100 (1978).

<sup>5</sup>D. H. E. Gross and J. Wilczynski, *Phys. Lett.* **67B**, 1 (1977).

<sup>6</sup>C. K. Gelbke, M. Bini, Colmer, D. L. Hendrie, J. L. Laville, J. Mahoney, M. C. Mermaz, D. K. Scott, and H. H. Wieman, *Phys. Lett.* **71B**, 83 (1977).

<sup>7</sup>D. C. Slater, J. R. Hall, J. R. Calareo, B. A. Watson, and J. A. Becker, *Phys. Rev. Lett.* **33**, 784 (1974).

<sup>8</sup>C. E. Anderson, in *Proceedings of the Second Conference on Reactions Between Complex Nuclei, Gatlinburg, Tennessee, 1960*, edited by A. Zucker, F. T. Howard, and E. C. Halbert (Wiley, New York, 1960), p. 67.

<sup>9</sup>R. W. Ollerhead, C. Chasman, and D. A. Bromley, *Phys. Rev.* **134** (1964).

<sup>10</sup>G. C. Morrison, *Phys. Rev. Lett.* **5**, 565 (1960).

<sup>11</sup>J. R. Pizzi, R. Bouche, M. Gaillard, P. Gaillard, A. Guichard, M. Gusakov, J. L. Leonhardt, and C. Ruhla, *Nucl. Phys.* **A136**, 496 (1969).

<sup>12</sup>J. S. Watson, H. G. Pugh, P. G. Roos, D. A. Goldberg, R. A. Riddle, and D. I. Bonbright, *Nucl. Phys.* **A172**, 513 (1972).

<sup>13</sup>A. K. Jain, J. Y. Grossiord, M. Chevallier, P. Gaillard, A. Guichard, M. Gusakov, and J. R. Pizzi, *Nucl. Phys.* **A216**, 519 (1973).

<sup>14</sup>D. Bachelier, M. Bernas, C. Detraz, R. Radvanyi, and M. Roy, *Phys. Lett.* **26B**, 283 (1968).

<sup>15</sup>P. G. Roos, D. A. Goldberg, N. S. Chant, and R. Woody III, *Nucl. Phys.* **A257**, 317 (1976).

<sup>16</sup>M. F. Werby, M. B. Greenfield, K. W. Kemper, D. L. McShan, and Steve Edwards, *Phys. Rev. C* **8**, 106

- (1973).
- <sup>17</sup>O. Häusser, A. B. McDonald, T. K. Alexander, and A. J. Ferguson, *Phys. Lett.* **38B**, 75 (1972).
- <sup>18</sup>J. L. Québert, B. Frois, L. Marquez, G. Sousbie, R. Ost, K. Bethge, and G. Gruber, *Phys. Rev. Lett.* **32**, 1136 (1974).
- <sup>19</sup>K. P. Artemov, V. Z. Goldberg, I. P. Petrov, V. P. Rudakov, I. N. Serikov, and V. A. Timofeev, *Yad. Fiz.* **21**, 1157 (1975) [*Sov. J. Nucl. Phys.* **21**, 597 (1975)].
- <sup>20</sup>K. P. Artemov, V. Z. Goldberg, I. P. Petrov, V. P. Rudakov, V. A. Timofeev, R. Wolskland, and J. Schmi-der, *Yad. Fiz.* **21**, 1169 (1975) [*Sov. J. Nucl. Phys.* **21**, 603 (1975)].
- <sup>21</sup>M. E. Cobern, *Phys. Rev. C* **14**, 491 (1976).
- <sup>22</sup>G. E. Moore and K. W. Kemper, *Phys. Rev. C* **14**, 977 (1976).
- <sup>23</sup>R. Ost, K. Bethge, H. Gemmeke, L. Lassen, and D. Scholz, *Z. Phys.* **266**, 369 (1974).
- <sup>24</sup>K. O. Pfeiffer, E. Speth, and K. Bethge, *Nucl. Phys.* **A206**, 545 (1973).
- <sup>25</sup>D. L. Disdier, G. C. Ball, O. Häusser, and R. E. Warner, *Phys. Rev. Lett.* **27**, 1391 (1971).
- <sup>26</sup>J. M. Hansteen and H. Wittern, *Phys. Rev.* **134**, B524 (1965).
- <sup>27</sup>H. Wittern, *Fortschr. Phys.* **14**, 401 (1966).
- <sup>28</sup>K. Bethge and K. Meier-Ewert, *Phys. Rev. Lett.* **18**, 1010 (1967).
- <sup>29</sup>H. W. Wittern, *Phys. Lett.* **32B**, 441 (1970).
- <sup>30</sup>W. H. Bassichis and A. Dar, *Phys. Rev. Lett.* **14**, 648 (1965).
- <sup>31</sup>A. A. Oglobin, *Fiz. Elem. Chastits At. Yadra* **3**, 936 (1972) [*Sov. J. Part. Nucl.* **3**, 467 (1973)].
- <sup>32</sup>A. I. Titov, *Yad. Fiz.* **19**, 292 (1974) [*Sov. J. Nucl. Phys.* **19**, 143 (1974)].
- <sup>33</sup>R. L. Gluckstern and G. Breit, in *Proceedings of the Second Conference on Reactions Between Complex Nuclei, Gallinburg, Tennessee, 1960*, edited by A. Zucker, F. T. Howard, and E. C. Halbert (Wiley, New York, 1960), p. 77.
- <sup>34</sup>H. Freiesleben, H. C. Britt, J. Birkelund, and J. R. Huizenga, *Phys. Rev. C* **10**, 245 (1974).
- <sup>35</sup>R. Broda, M. Ishihara, B. Herskind, H. Oeschler, S. Ogaza, and H. Ryde, *Nucl. Phys.* **A248**, 356 (1975).
- <sup>36</sup>J. Kropp, H. Klewe-Nebenius, J. Bushmann, H. Rebel, H. Faust, H. J. Gils, J. Reider, and K. Wisshak, *Z. Phys.* **A280**, 61 (1977).
- <sup>37</sup>C. M. Castaneda, H. A. Smith, Jr., T. E. Ward, and T. R. Nees, *Phys. Rev. C* **16**, 1437 (1977).
- <sup>38</sup>J. G. Fleissner, D. A. Rakel, F. P. Venezia, E. G. Funk, J. W. Mihelich, and H. A. Smith, Jr., *Phys. Rev. C* **17**, 1001 (1978).
- <sup>39</sup>C. M. Castaneda *et al.*, *Bull. Am. Phys. Soc.* **22**, 1003 (1978).
- <sup>40</sup>C. M. Castaneda *et al.*, *Bull. Am. Phys. Soc.* **23**, 540 (1978).
- <sup>41</sup>C. M. Castaneda, H. A. Smith, Jr., P. P. Singh, J. Jastrzebski, H. Karwowski, and A. K. Gaigalas, *Phys. Lett.* **77B**, 371 (1978).
- <sup>42</sup>J. B. A. England, in *Techniques in Nuclear Struc-ture Physics* (Wiley, New York, 1974), p. 463 ff.
- <sup>43</sup>T. D. Thomas, *Phys. Rev.* **116**, 703 (1959).
- <sup>44</sup>M. Blann, University of Rochester Report No. COO-3494-29, 1976 (unpublished).
- <sup>45</sup>W. Von Oertzen, in *Nuclear Spectroscopy and Reactions*, Part B, edited by J. Cerny (Academic, New York, 1974), p. 279.
- <sup>46</sup>S. E. Vigdor *et al.*, *Bull. Am. Phys. Soc.* **22**, 1003 (1977), and private communication.
- <sup>47</sup>W. Norenberg and H. A. Weidenmuller, in *Lecture Notes in Physics*, No. 51 (Springer, Berlin, 1976), p. 45.
- <sup>48</sup>Y. Sakamoto, P. Cuer, and F. Takeutchi, *Phys. Rev. C* **9**, 2440 (1974).
- <sup>49</sup>H. Karwowski, Indiana University, private communi-cation.
- <sup>50</sup>N. Austern, *Direct Nuclear Reaction Theories* (Wiley, New York, 1970), p. 115.
- <sup>51</sup>D. Proetl, R. M. Diamond, and F. S. Stephens, *Nucl. Phys.* **A231**, 301 (1974).
- <sup>52</sup>R. M. Lieder, A. Leskakis, M. Muller-Veggian, Y. Gono, C. Mayer-Böricke, S. Beshai, K. Fransson, C. G. Linden, and Th. Lindblad, *Nucl. Phys.* **A299**, 255 (1978).
- <sup>53</sup>A. Chevarier, N. Chevarier, T. M. Duc, and J. Tousset, *C. R. Acad. Sci. (Paris) Ser. B* **270**, 182 (1970).
- <sup>54</sup>H. E. Kurz, E. W. Jasper, K. Fisher, and F. Her-mes, *Nucl. Phys.* **A168**, 129 (1971).
- <sup>55</sup>G. D. Dracoulis, private communication.
- <sup>56</sup>Yu. V. Khrisanfov, V. Yu. Padalko, and P. P. Zarubin, *Izv. Akad. Nauk Ser. Fiz.* **36**, 641 (1972); *Bull. Acad. Sci. USSR, Phys. Ser.* **36**, 580 (1972).
- <sup>57</sup>P. Jahn, H. J. Probst, A. Djalois, W. F. Davidson, and C. Mayer-Böricke, *Nucl. Phys.* **A209**, 333 (1973).
- <sup>58</sup>K. S. Krane *et al.*, *Nucl. Data Tables* **11**, No. 5, 351 (1973).
- <sup>59</sup>R. M. Steffen and K. Alder, in *Electromagnetic In-teraction in Nuclear Spectroscopy*, edited by W. D. Hamilton (North-Holland, Amsterdam, 1975), Ch. XII.
- <sup>60</sup>C. M. Castaneda, Ph.D. dissertation, 1978 (unpub-lished), also available as Indiana University Cyclo-tron Facility (IUCF) Internal Report No. 78-01, 1978.
- <sup>61</sup>D. Scholz, H. Gemmeke, L. Lassen, R. Ost, and K. Bethge, *Nucl. Phys.* **A288**, 351 (1977).
- <sup>62</sup>D. Kunz, (DWUCK), DWBA Code, Version 4 (1974).
- <sup>63</sup>R. Huffman, A. Galonsky, and R. G. Markham, Uni-versity of Michigan Annual Report, 1977, p. 28 (un-published).
- <sup>64</sup>K. Alder, A. Bohr, T. Huus, B. Mottelson, and A. Winther, *Rev. Mod. Phys.* **28**, 77 (1956).
- <sup>65</sup>R. Serber, *Phys. Rev.* **72**, 1008 (1947).
- <sup>66</sup>C. K. Gelbke *et al.*, *Phys. Lett.* **70B**, 415 (1977).
- <sup>67</sup>J. R. Wu, C. C. Chang, and H. D. Holmgren, *Phys. Rev. Lett.* **40**, 1013 (1978).
- <sup>68</sup>H. Gemmeke, B. Deluigi, L. Lassen, and D. Scholz, *Z. Phys.* **A286**, 73 (1978).
- <sup>69</sup>F. Ajzenberg-Selove and T. Lauritsen, *Nucl. Phys.* **A227**, 1 (1974).